Root associated *Streptomyces* produce galbonolides to modulate plant immunity and promote rhizosphere colonisation

Clément Nicolle[1], Damien Gayrard[1,2], Alba Noël[3], Marion Hortala[1], Aurélien Amiel[2], Sabine Grat-Simeone[1], Aurélie Le Ru[4], Guillaume Marti[1,5,6], Jean-Luc Pernodet[3], Sylvie Lautru[3], Bernard Dumas[1*], Thomas Rey[2*]

AFFILIATIONS

[1] Laboratoire de Recherche en Sciences Végétales, Université de Toulouse, CNRS, Université Toulouse III, Toulouse INP, 24 Chemin de Borde Rouge, Auzeville, 31320, Auzeville-Tolosane, France

[2] DE SANGOSSE, Bonnel, 47480, Pont-Du-Casse, France

[3] Université Paris-Saclay, CEA, CNRS, Institute for Integrative Biology of the Cell (I2BC), 91198, Gif-sur-Yvette, France

[4] Plateforme d'Imagerie FRAIB-TRI, Université de Toulouse, CNRS, Auzeville-Tolosane 31320, France

[5] Metatoul-AgromiX Platform, LRSV, Université de Toulouse, CNRS, UPS, Toulouse INP, Toulouse, France,

[6] MetaboHUB-MetaToul, National Infrastructure of Metabolomics and Fluxomics, Toulouse, France

***Contributed equally**

CORRESPONDING AUTHOR'S EMAIL

bernard.dumas@univ-tlse3.fr

reyt@desangosse.com

LEAD CONTACT

Further information and requests for resources and reagents should be directed to the lead contact Thomas Rey. reyt@desangosse.com

ABSTRACT

The rhizosphere, which serves as the primary interface between plant roots and the soil, constitutes an ecological niche for a huge diversity of microbial communities. Currently, there is little knowledge on the nature and the function of the different metabolites released by rhizospheric microbes to facilitate colonization of this highly competitive environment. Here, we demonstrate how the production of galbonolides, a group of polyene macrolides that inhibit plant and fungal Inositol Phosphorylceramide Synthase (IPCS), empowers the rhizospheric *Streptomyces* strain AgN23, to thrive in the rhizosphere by triggering the plant's defence mechanisms. Metabolomic analysis of AgN23-inoculated *Arabidopsis* roots revealed a strong induction in the production of an indole alkaloid, camalexin, which is a major phytoalexin in *Arabidopsis*. By using a plant mutant compromised in camalexin synthesis, we show that camalexin production is necessary for the successful colonization of the rhizosphere by AgN23. Conversely, hindering galbonolides biosynthesis in AgN23 knock-out mutant resulted in loss of inhibition of IPCS, a deficiency in plant defence activation, notably the production of camalexin, and a strongly reduced development of the mutant bacteria in the rhizosphere. Together, our results throw light on the mechanism by which streptomycetes induce the production of a root defence compound to support their colonisation of the rhizosphere.

INTRODUCTION

Cross-kingdom communications play a significant role in shaping interactions between organisms within diverse ecological niches[1]. Microbe-microbe communication is often mediated by the secretion of small and diffusible specialised metabolites [2-6]. Throughout their lifecycle, eukaryotic organisms such as plants, are known to associate with the abundant and diverse community of microorganisms[7-9]. However, there is currently limited knowledge on how plants establish communication with microorganisms and regulate their populations in and around their tissues[10]. It has been noted that plants, even when grown in contrasted soils, tend to assemble a core microbiota comprising bacteria, fungi and oomycetes, suggesting the existence of broad trans-kingdom communication mechanisms

49 within plant-microbe interactions[11]. In this context, it becomes primordial to understand the
50 molecular basis of plant-microbiota assembly to achieve the intelligent engineering of crops
51 microbiota[12]. Such approach would be an important milestone towards sustainable agricultural
52 practices in nutrition and protection against pathogens and abiotic stresses [13,14]. An example of this
53 approach is the recently reported study on how a *Streptomyces* strain alleviates abiotic stress in a
54 plant by producing single specialised metabolites[15].

55 The *Streptomyces* genus belongs to Actinobacteria, a family of filamentous sporulating Gram+
56 bacteria which constitutes the second most prominent component of root microbiota after
57 proteobacteria[16,17]. Among Actinobacteria, *Streptomyces* spp. are enriched in endophytic and
58 epiphytic root compartments and represent up to 30% of the total bacterial OTUs[18]. Enrichment of
59 *Streptomyces* spp. in soil and rhizosphere correlates with resistance to drought and pathogen
60 attack[7,19]. Furthermore, streptomycetes are hallmark producers of antibiotic specialised metabolites
61 involved in protection against plant pathogens [20-22]. *Streptomyces* spp. have also been demonstrated
62 to elicit Salicylic Acid (SA) and ISR dependent responses leading to the activation of plant defence
63 metabolism[23,24]. These important attributes have stimulated great interest in the use of
64 streptomycetes for crop protection [25,26].

65 In a previous paper, we reported the screening of a collection of 35 *Streptomyces* strains isolated
66 from agricultural soils for their plant defence elicitation[27]. Among these, the AgN23 strain has been
67 reported to display a remarkable potential to elicit *Arabidopsis* defences associated to salicylate,
68 jasmonate and ethylene signalling[27]. Foliar inoculation with the bacteria resulted in the formation of
69 *SALICYLIC INDUCTION DEFICIENT 2 (SID2)* dependent necrotic symptoms in *Arabidopsis* and protection
70 against *Alternaria brassicicola* colonisation. A recent analysis of the AgN23 genome showed that the
71 strain belongs to the rhizospheric clade *S. violaceuniger* [28]. The AgN23 genome harbours large gene
72 families associated to rhizosphere colonization, such as biosynthetic gene clusters (BGCs) involved in

73 the synthesis of plant bioactive and antimicrobial compounds, plant cell wall degrading enzymes, and
74 phytohormone synthesis.

75 In this work, we investigate the molecular basis of AgN23 interaction with plant roots. We set up
76 inoculation assays of AgN23 with *Arabidopsis* roots and characterised both the rhizosphere
77 colonisation by the bacteria and the resulting plant responses. We find that AgN23 triggered a rewiring
78 of the root metabolome resulting in the production of the antimicrobial camalexin and we show that
79 the production of this phytoalexin is an important feature of AgN23 rhizosphere colonisation. We then
80 went on to investigate whether specialised metabolites of AgN23 are involved in rhizosphere
81 colonisation and identified several polyketides that are known to inhibit the plant and fungal Inositol
82 Phosphorylceramide synthases (IPCS), enzymes involved in the sphingolipid metabolism. We built
83 AgN23 knock out mutants in the AgN23 galbonolides BGC and showed that the resulting mutants were
84 severely compromised in plant defence stimulation and rhizosphere colonisation suggesting
85 galbonolides act as major signals to promote AgN23 proliferation in the rhizosphere through the
86 induction of camalexin production.

87 **RESULTS**

88 **AgN23 colonises *Arabidopsis* rhizodermis and rhizosphere**

89 In view of the fact that AgN23 was isolated from grapevine rhizosphere, we looked into the interaction
90 of the strain with roots by inoculating *in vitro* grown *Arabidopsis thaliana* Col-0 seedlings with AgN23
91 spores. A drop of the spore suspension was deposited at the root tip of young seedlings. A strong
92 development of bacterial microcolonies was observed at the inoculation site 10 days after inoculation
93 (Figure 1a). We generated GFP and RFP-labelled transgenic AgN23 strains and observed the
94 colonization patterns of both strains by epifluorescence microscopy. Results showed that bacteria can
95 spread beyond the initial inoculation spot and colonise other developing sections of the root system,
96 such as lateral roots and apical meristem (Figure 1b). Visual and microscopic inspection of the AgN23-
97 treated plants suggested that the inoculated bacteria did not lead to any characteristic symptoms such

98 as root browning or rhizodermis damages in Arabidopsis. Moreover, penetration of AgN23 into the
99 root tissues was not observed. Nevertheless, we observed that AgN23 inoculation did result in a slight
100 (about 10%) reduction in root elongation (Figure 1c).

101 To study the colonization of the rhizosphere by AgN23, we inoculated potting soil with 10^5 AgN23
102 spores/g of soil prior to sowing Arabidopsis seeds. Consistent with our previous *in vitro* observation,
103 the presence of AgN23 reduced rosette growth without causing obvious symptoms to the leaves
104 (Figure 1d, 1e). The development of AgN23 in the inoculated soil was monitored by extracting
105 microbial DNA from both unplanted and rhizosphere soil samples. A total of 3.06×10^8 genome copies
106 of AgN23 were detected in the unplanted soil 7 weeks post inoculation, whereas 1.87×10^{10} genome
107 copies of the bacteria were detected in the rhizosphere. This shows that AgN23 preferentially
108 colonised the Arabidopsis rhizosphere rather than the unplanted soil (Figure 1F). Taken together, our
109 data confirm that AgN23 is an epiphytic and rhizospheric bacterium that triggers plant growth
110 inhibition, albeit without symptoms.

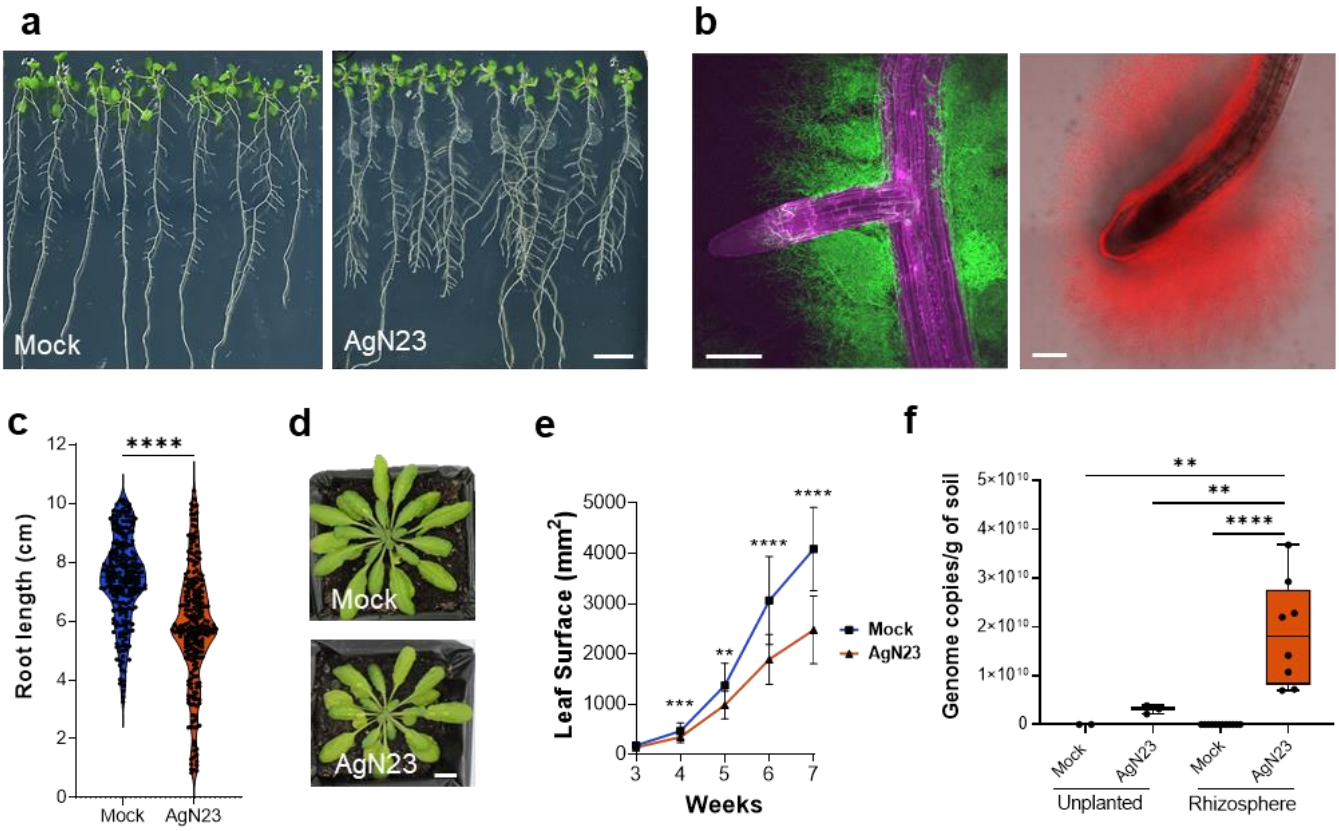

Figure 1: AgN23 colonizes rhizoplane and rhizosphere of *Arabidopsis thaliana* and slightly inhibits plant growth. a. Observation of *A. thaliana* Col-0 colonization by AgN23 at 10 days after inoculation with spores at the root apex. Scale bar = 1 cm. **b.** Confocal fluorescence images of AgN23-mCherry (red) colonizing root apical meristem and AgN23-GFP (green) developing around lateral root. Scale bars: 250 µm **c.** Primary root length of *Arabidopsis* seedlings 10 days after inoculation with AgN23 spores at the root apex from Violin plots created from data from 30 independent assays each involving at least 10 plants per treatment (n = 300). The whiskers encompass the minimum and maximum values, and the midline shows the median. Statistical differences between the treatments were analyzed using Mann–Whitney test and '****' represents significant differences at $p < 0.0001$. **d.** Typical photographs of 6-week- old Arabidopsis rosettes following growth within non- or inoculated potting soil. Scale bar: 1 cm. **e.** Leaf area measurement of *Arabidopsis* rosettes grown in AgN23-inoculated potting soil. Graphs show the mean ± SD calculated from at least eight biological replicates (n = 8). Statistical comparison between inoculation and mock conditions was performed based on T-test ('**' = $p < 0.01$; '***' = $p < 0.001$; '****' = $p < 0.0001$). **f.** AgN23 genome copy number in *Arabidopsis* rhizosphere 4 and 8 weeks after soil inoculation. Box plots were created from data involving at least 8 plants per treatment (n = 8). Whiskers encompass the minimum and maximum values, and the midline shows the median. Statistical differences between the treatments were analyzed using Mann–Whitney test; '****' and '**' represent significant differences at $p < 0.0001$ and $p < 0.05$, respectively.

Activation of camalexin biosynthesis by AgN23 promotes bacteria settlement in the rhizosphere

In a previous work, we characterised the plant defence stimulating activity of AgN23 and found that the bacterial culture media extract (CME) induced robust transcriptional responses associated with *Arabidopsis* specialized metabolism[27]. Detailed analysis showed transcriptional induction of genes coding enzymes involved in camalexin biosynthesis following treatment with AgN23 CME after 1 and 6 h post-treatment (Figure S1).

a

Id	Name	AgN23 1 hpi	AgN 23 6 hpi
at5g60890	ATMYB34	-1.689	-1.77
at1g18570	MYB51	4.54	5.32
at1g74080	ATMYB122	12.378	14.321
at4g39950	CYP79B2	-1.093	5.684
at4g31500	CYP83B1	-1.075	2.754
at2g30750	CYP71A12	18.592	55.686
at2g30770	CYP71A13	-1.294	153.13
at3g26830	PAD3	28.805	29.805

b

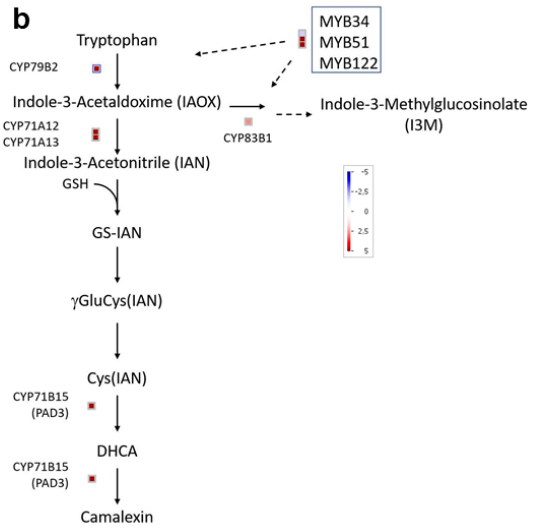

138 **Figure S1:** Expression of genes involved in the biosynthesis of indolic compounds following treatment
139 of *Arabidopsis* seedlings with AgN23 CME. Transcriptomic data from Vergnes et al., 2020 were mined
140 to extract expression of genes falling in the category of indolic biosynthesis. **a.** Fold induction or
141 repression expressed in Log2 of genes involved in gene regulation (MYB factors) or camalexin
142 biosynthesis at 1 hour post inoculation (hpi) and 6 hpi. **b.** Mapman display of gene regulation at 6 hpi
143 from the biosynthesis pathway of camalexin and I3M (adapted from Ferigmann et al., MPMI Vol. 34,
144 No. 5, 2021, pp. 560–570).

145 To analyse the metabolomic response of root tissues to AgN23, we extracted the metabolites from
146 whole seedlings cultivated *in vitro* in contact with AgN23 for 10 days, which were then characterized
147 by a full-scan LC-HRMS metabolomics analysis. Samples were injected, analysed with ESI+ and ESI-
148 modes, and combined in a single list of variables. A total of 511 variables were retrieved across all the
149 samples out of which, 416 received level 3 annotations according the Metabolomic Standard Initiative
150 based on internally built database and the exact mass and fragmentation profile of the ions (Data S1).
151 Unsupervised PCA of the complete variable dataset allowed us to clearly discriminate the control
152 samples from those inoculated with AgN23, with component 1 and component 2 supporting 32.9 %
153 and 21.6% of the variability, respectively (Figure S2).

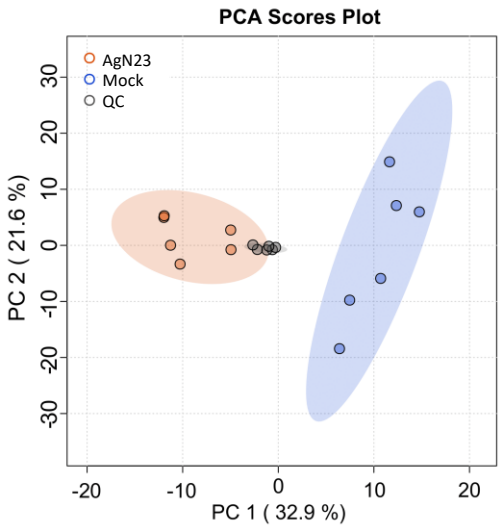

154

155 **Figure S2:** PCA score plot of UHPLC-HRMS data (n = 511 variables) from extracts of *Arabidopsis*
156 *thaliana* 10 days after inoculation or not with AgN23 spores. QC: quality control

157

158

159 To identify the underlying chemical classes supporting the separation of control and AgN23 inoculated
160 samples, we computed the fold change for each individual variable between the two conditions.
161 Results showed that 20 and 39 metabolites were enriched in control and AgN23 conditions,
162 respectively (Data S1). These metabolites were sorted based on their chemical classes, revealing a
163 strong induction of metabolites belonging to specialised metabolism, such as indoles, flavonoids or
164 fatty acyls (Figure 2a). A PLS-DA model was then built to identify the most significant metabolites
165 supporting samples separation (Figure 2b). It turned out that primary metabolism markers (sucrose
166 and glutamate) were enriched in the control root, suggesting that these are depleted from the roots
167 in presence of the bacteria. In contrast, camalexin and indol-3-yl-methylglucosinolate (I3M) were the
168 two most significant enriched metabolites in AgN23 treated roots. This suggests that the biosynthesis
169 of these two metabolites is induced by the bacteria. This conclusion was further substantiated by
170 comparing the peak areas corresponding to the two metabolites in mock and AgN23 treated plants.
171 In the presence of AgN23, 259.4 and 2.2-fold induction were noted for camalexin and I3M, respectively
172 (Figure 2c).

173 In view of the strong and specific production of camalexin in response to AgN23, we characterised
174 the behaviour of the *phytoalexin deficient mutant 3 (pad3-1),* mutated in a CYP450 coding gene which
175 converts cysteine-indole-3-acetonitrile to camalexin, in response to the bacteria[29]. Metabolomics
176 characterisation of *pad3-1* roots indicated that the metabolome of *pad3-1* upon AgN23 inoculation
177 xas indistinguishable from that under mock conditions (Figure 2d, Data S2). We further validated the
178 complete lack of induction of camalexin biosynthesis in *pad3-1* (figure 2e).

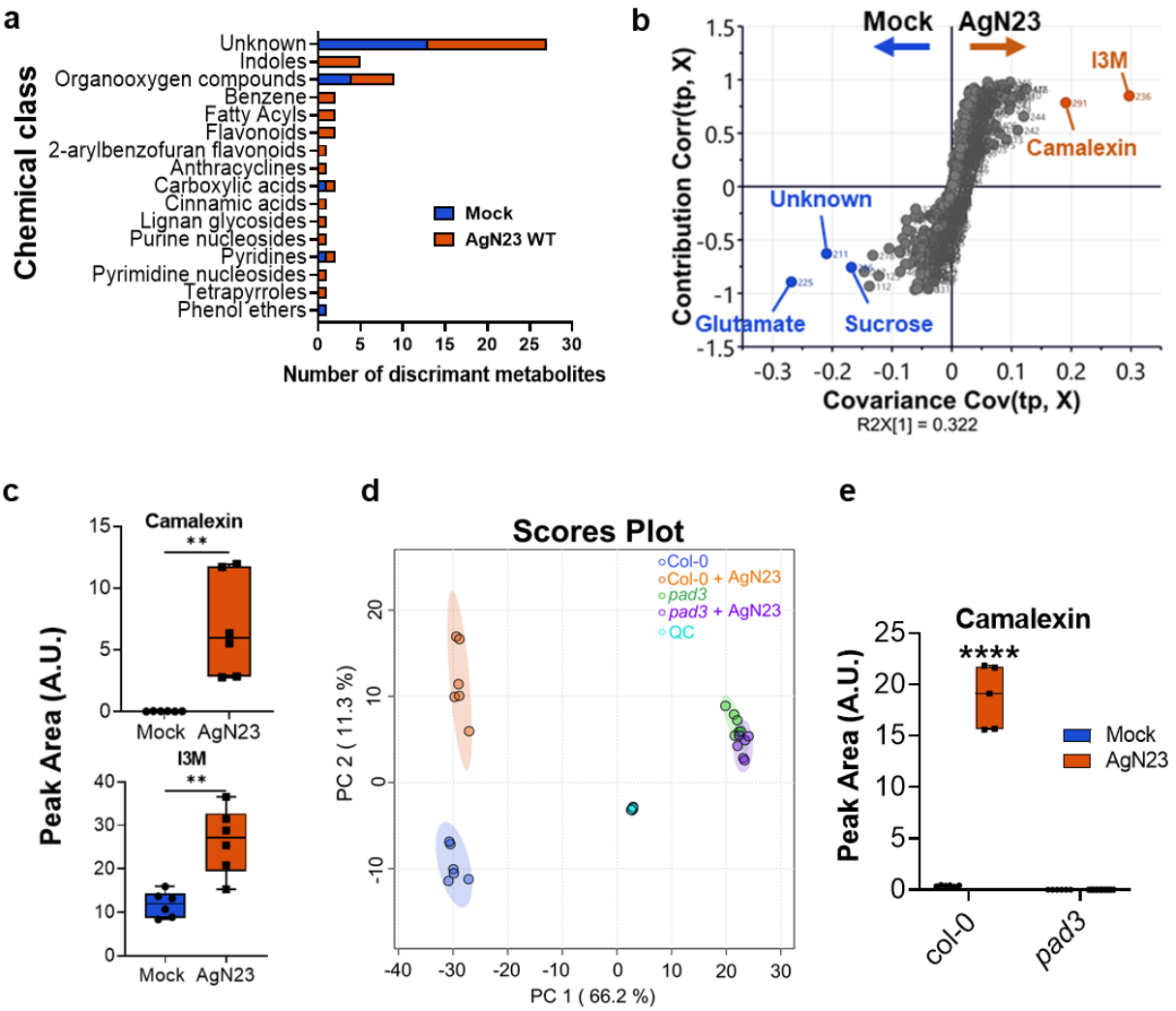

Figure 2: AgN23 induces camalexin biosynthesis in *Arabidopsis* roots. a. Discriminant metabolites overrepresented in mock or AgN23 treated *Arabidopsis* roots based on UHPLC-MS profiling data. The metabolites are displayed as chemical classes, determined with Classyfire, using the criteria of $p < 0.05$ (T-test, control vs treatment, unadjusted p-value) and log2 fold change (log2FC) > 0.8 or < -0.8. **b.** Corresponding S-plot of OPLS-DA score plot based on Mock vs AgN23 comparison (n = 511 variables, the OPLS-DA model was validated by a permutation test with 200 counts). The variables with VIP > 3.5 are indicated by orange and blue filled circles for AgN23 group and mock group, respectively. c. Average peak area of the 2 biomarkers significantly induced in AgN23 treated roots (VIP > 3.5). Box plots were created from data from six independent assays (n = 6). The whiskers encompass the minimum and maximum values, and the midline shows the median. Statistical differences between the treatments were analyzed using unpaired T-test and '**' represents significant differences at $p < 0.01$. I3M: indole-3-yl-methyl. **d.** PCA score plot of UHPLC-MS data (n = 534 variables) from extracts of *Arabidopsis* Col-0 or *pad3-1* 10 days after inoculation with AgN23. **e.** Average peak area of camalexin. Box plots were created from data from six independent assays (n = 6). The whiskers encompass the minimum and maximum values, and the midline shows the median.

195 Interestingly, we observed that *pad3-1* plants inoculated with AgN23 showed a phenotype similar
196 to that of the wild type Col-0 (Figure 3a, 3b) with respect to roots and rosette growth inhibitions
197 (Figure 3c, 3d). To check if camalexin production had any effect on AgN23 multiplication in the
198 rhizosphere, we quantified AgN23 in the rhizosphere of the WT and the *pad3-1* mutant. Results
199 showed that the number of genome copies of AgN23 in the rhizosphere of *pad3-1* plant was
200 significantly lower than in Col-0 (Figure 3e). Taken together with the data from *in vitro* inoculation,
201 these results demonstrate that the induction of camalexin synthesis promotes AgN23 colonisation in
202 the rhizosphere.

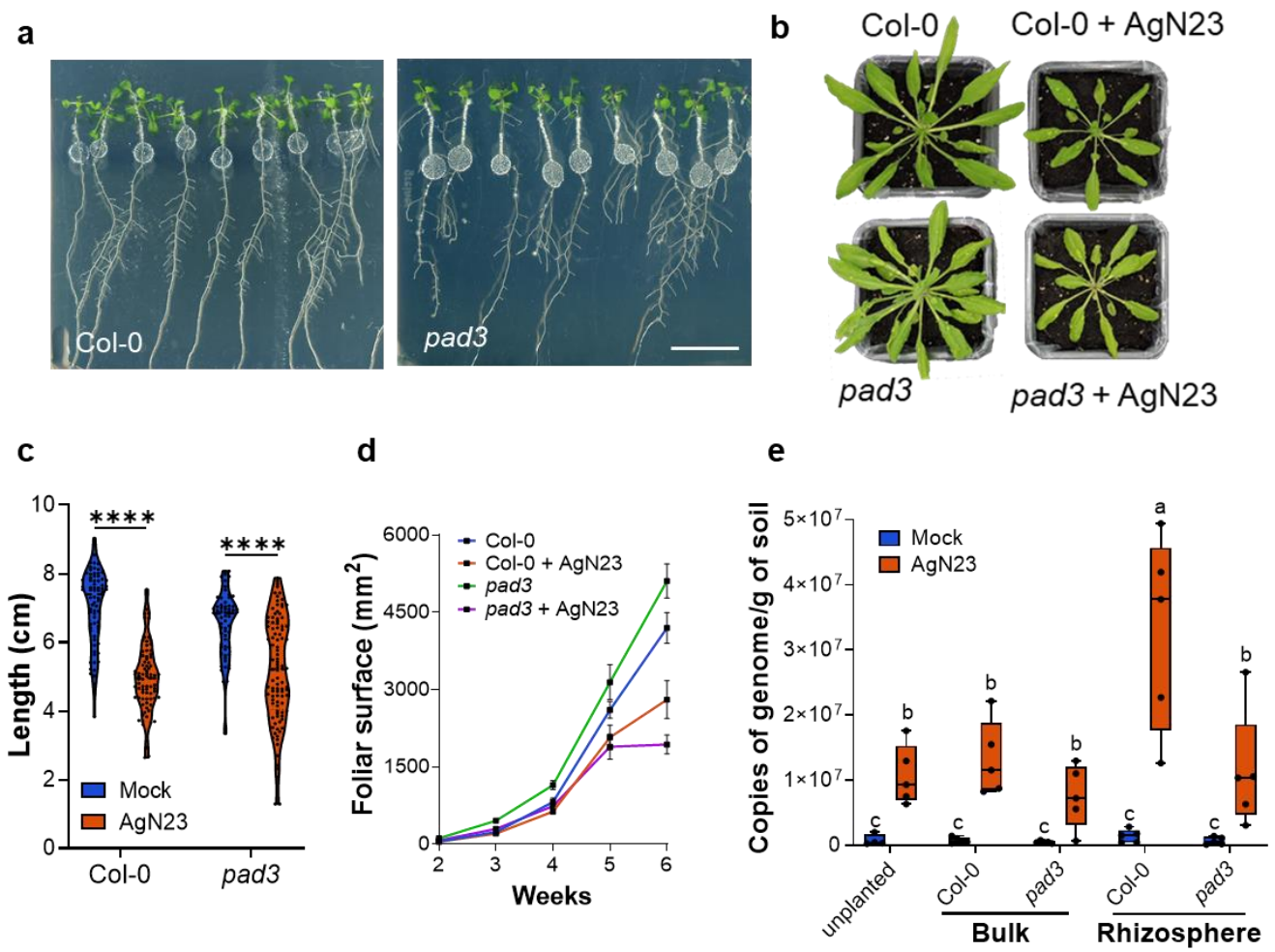

203 **Figure 3: Biosynthesis of camalexin enables enrichment of AgN23 in the *Arabidopsis* rhizosphere. a.**
204 Observation of *A. thaliana* Col-0 and *pad3-1* colonization by AgN23 at 10 days after inoculation with
205 spores at the root apex. Scale bar = 2 cm **b.** Rosette development of the plants Col-0 and *pad3-1* after
206 inoculation with AgN23 spores. Typical photographs of 6-week-old col-0 or pad3 rosettes are shown.
207 **c.** Primary root length of plants colonized or not by AgN23 at 10 days after inoculation. **d.** Leaf area
208 measurement. Graphs show the mean ± SD calculated from at least eight biological replicates (n = 8).

209 **e.** AgN23 genome copy number in Col-0 or *pad3-1 Arabidopsis* rhizosphere 6 weeks after soil
210 inoculation with AgN23. Box plots were created from data from 5 plants per treatment (n = 5). The
211 whiskers encompass the minimum and maximum values, and the midline shows the median. Letters
212 a to c represent statistical differences between the treatments based on 2-way ANOVA followed by
213 Tukey's multiple comparisons test.

214

215 **AgN23 produces galbonolides, polyketides capable of inhibiting plant inositol phosphorylceramide**

216 **synthase**

217 To identify AgN23 specialised metabolites that could be involved in elicitation of root metabolome
218 responses, we performed a LC-HRMS global metabolomics analysis. Briefly, apolar compounds of the
219 CME were adsorbed on XAD16 resin beads and extracted with butanol prior to preparation for full-
220 scan liquid chromatography high-resolution mass spectrometry (LC-HRMS). The samples were
221 injected in ESI+ and ESI- mode and combined in a single list of variables. A total of 1022 variables were
222 retrieved across all the samples and 812 received level 3 annotations according the Metabolomic
223 Standard Initiative based on internally built database and the exact mass and fragmentation profile of
224 the ions (Data S3). This approach led to the putative identification of several specialised metabolites
225 that have been known to be produced by *Streptomyces* ssp. (Figure S3, Table 1).

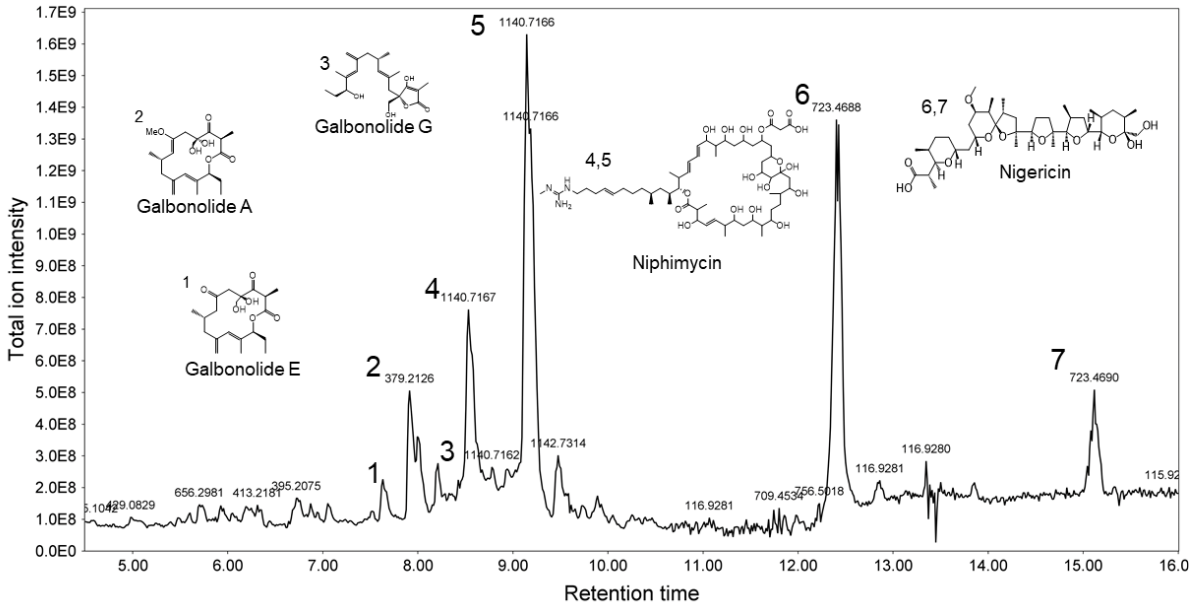

226

227 **Figure S3:** UHPLC-HRMS chromatogram of AgN23 CME expressed in Total Ion Intensity. Peaks with
228 the highest intensities were annotated with putative structures based on HRMS and MS/MS spectra.

229 Among these specialised metabolites, we identified the antifungal compounds niphimycin,
230 nigericin and galbonolides (also known as rustmicin). The identification of these specialised candidate
231 metabolites is consistent with the biosynthetic gene clusters (BGCs) that we recently annotated[28].
232 Among the three compounds, galbonolides were originally reported for their inhibitory activities
233 against fungal and in plants inositol phosphorylceramide synthase (IPCS), an enzyme involved in the
234 metabolism of sphingolipids[30]. The loss of function of an IPCS gene in *Arabidopsis* has been shown to
235 be associated with programmed cell death linked to defence mechanisms[31-36]. Given that the inhibition
236 of plant IPCS can trigger SA-dependent HR-like lesions, such as those observed in response to AgN23
237 CME, we decided to study the implication of galbonolides in *Arabidopsis* responses to AgN23[27]. We
238 constructed AgN23 knock out mutants in the polyketide synthase of the galbonolides BGCs by
239 disrupting the *galB* gene (S97_41300) (Figure 4a). Galbonolides detection was fully abolished in the
240 CME of galbonolides knock-out mutants (Figure 4b). This finding confirmed the function of the
241 predicted galbonolide gene cluster in the synthesis of all the galbonolides detected (galbonolides A,
242 B, E and G).

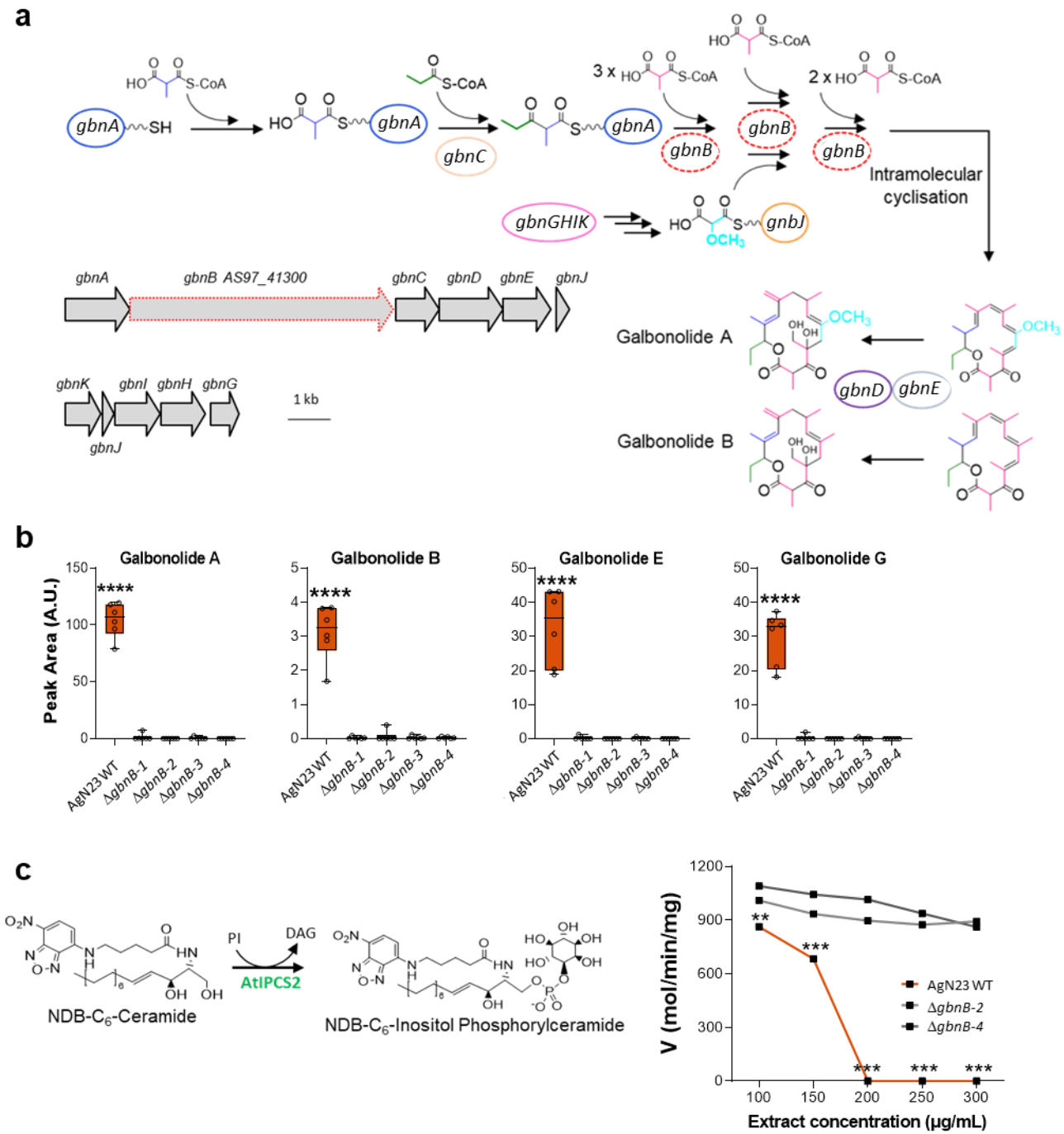

Figure 4: AgN23 produces galbonolides, a class of macrolides capable of inhibiting plant Inositolphosphoryl Ceramide Synthase. a. Biosynthesis pathway of galbonolides (*gbn*A-E) and of methoxymalonyl-CoA (*gbn*H-K) in AgN23. The targeted locus of the AgN23 galbonolide BCG for knock-out is shown by the red broken line (NCBI locus tags from assembly GCA_001598115.2). **b.** Average peak area of the different putative galbonolides structures detected in AgN23 Culture Media Extract based on HRMS and MS/MS spectra. Box plots were created from data from 6 biological replicates (n = 6). The whiskers encompass the minimum and maximum values, and the midline shows the median. Statistical differences between the AgN23 wild-type (WT) group and the AgN23 KO (Δ*gbnB*) groups were analyzed using one-way analysis of variance (ANOVA) and Tukey's HSD test (α = 0.05) and '****'

253 represents significant differences at p < 0.0001. **c.** Pathway of of NBD-C6-ceramide to NBD-C6-IPC
254 conversion by the *Arabidopsis* Inositolphosphoryl Ceramide Synthase (AtIPCS2) and enzyme activity
255 following treatments with butanol extracts from culture supernatant of AgN23 WT or KO mutants
256 (Δ*gbnB*-2 and Δ*gbnB-4*). Graphs show the mean ± SD calculated from 6 independent assays (n = 6).
257 Statistical differences between the AgN23 wild-type (WT) group and the AgN23 KO (Δ*gbnB*) groups
258 were analyzed using multiple Mann-Whitney test (FDR = 1%) and '***' and '**' represent p < 0.001
259 and p < 0.01, respectively.

260 To investigate the effect of AgN23 and galbonolide mutants CMEs on the IPCS activity, we prepared
261 a microsomal fraction from a *Saccharomyces cerevisiae* strain producing recombinant *Arabidopsis*
262 IPCS2 (AT2G37940)[37] and IPCS enzymatic activity was tracked by HPLC-Fluorescence method with the
263 fluorescent substrate NBD-C_6-ceramide[38]. We obtained for IPCS2 a Km of 7.57 fitting with previous
264 studies of the enzyme[37] (Figure S4).

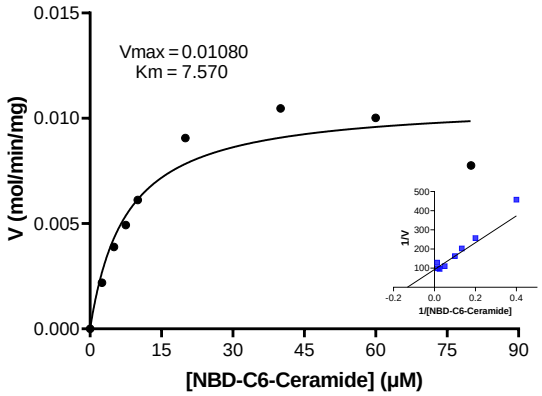

265

266 **Figure S4:** Michaelis-Menten and Lineweaver Burk Vmax, and Km estimations from enzyme assays of
267 the Inositolphosphoryl ceramide synthase from *Arabidopsis* thaliana (AtIPCS2). 0.1 mg/mL of total
268 microsomal membranes were used to study the conversion of and the NBD-C6-Ceramide to NBD-C6-
269 IPC. The fluorescence values of the assays were converted to concentrations based on the line of best
270 fit from the standard curve of NBD-C6-Ceramide (3–500 µM).

271

272 We then tested the enzymatic activity in presence of AgN23 and mutant CMEs in the concentration
273 range of 100– 300µg/ml. We observed that the AgN23 CME displayed a drastic inhibition of the
274 enzymatic activity at concentrations greater than 200µg/ml dilution (Figure 4c) whereas no such
275 inhibition was observed in the CME of two selected AgN23 galbonolides knock-out mutants (Δ*gbnB-2*
276 and Δ*gbnB-4*). Taken together, these data revealed that galbonolides secretion by AgN23 was the
277 driving factor in the inhibition of *Arabidopsis* IPCS2.

278 Complementarily, since galbonolides were originally described as antifungal metabolites, the
279 antifungal activity of the mutant was analysed against the filamentous fungus *Botrytis cinerea*[39,40]. As
280 expected, the loss of galbonolides in knock out mutants resulted in a reduced antifungal activity of the
281 CME (Figure S5, Table 2).

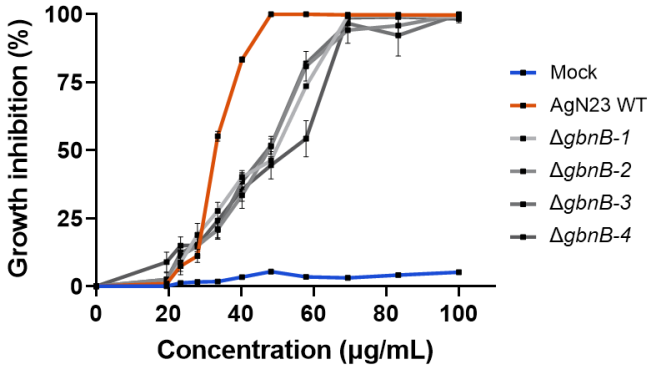

282 **Figure S5:** Growth inhibition of Botrytis cinerea following treatment with CME of AgN23 WT and
283 Δ*gbnB* mutants. Graphs show the mean ± SD calculated from six biological replicates (n = 6).
284

285 **Galbonolides are major contributors of the AgN23 eliciting activity and play a crucial role in**
286 **rhizosphere colonisation by AgN23**

287 In a previous work, we identified AgN23 as a *Streptomyces* strain producing strong elicitors of the
288 hypersensitive reaction (HR) including localised necrosis and expression of defence markers such as
289 *Pathogenesis Related 1 PR1)*, *Phytoalexin Deficient 4 (PAD4)* and *Phytoalexin Deficient 3 (PAD3)*[27].
290 Here, we investigated whether galbonolides may play important role in these responses to the
291 bacterium. Agroinfiltration of *Nicotiana benthamiana* leaves with AgN23 CME induced cell death at
292 50 µg/ml concentration while no sign of necrosis could be observed at the same concentration with
293 CMEs of the galbonolides mutants Δ*gbnB-2* and Δ*gbnB-4* (Figure 5a). It is noteworthy that similar
294 necrotic responses were observed when CME of the wild type and mutant strains were infiltrated at
295 200 µg/ml or higher concentrations, suggesting that other necrotic elicitors were produced by the
296 mutants. To investigate the effect of AgN23 CME on the necrotic responses of *Arabidopsis*, we
297 performed ion leakage assays from infiltrated leaf discs of *Arabidopsis* with the 4 independent

298 mutants of AgN23 and further confirmed the reduction in necrotic responses triggered by AgN23
299 when galbonolides biosynthesis is abolished (Figure 5b). Since variation of nuclear calcium
300 concentration is a typical signal associated with HR, we analysed the nuclear calcium concentration of
301 *Arabidopsis* plants following treatment using a line expressing a nuclear apo-aequorine reporter gene.
302 This reporter line was also selected based on a previous observation that a nuclear calcium signal
303 controls the apoptotic cell death induced by d-*erythro*-sphinganine, a compound related to the
304 sphingolipid pathway, in tobacco cells[41]. Luminescence quantification triggered by AgN23 CME in
305 hydroponically grown *Arabidopsis* peaked at 4 min post treatment and this signature was abolished in
306 the galbonolides mutants (Figure 5c). Similarly, we analysed by live imaging *Arabidopsis* seedlings
307 inoculated at the root tip with AgN23 CME and observed that this treatment resulted in a quick
308 activation (<15 min) of nuclear calcium signalling in the root tip which then spread to the entire root
309 plantlets (Figure 5d).

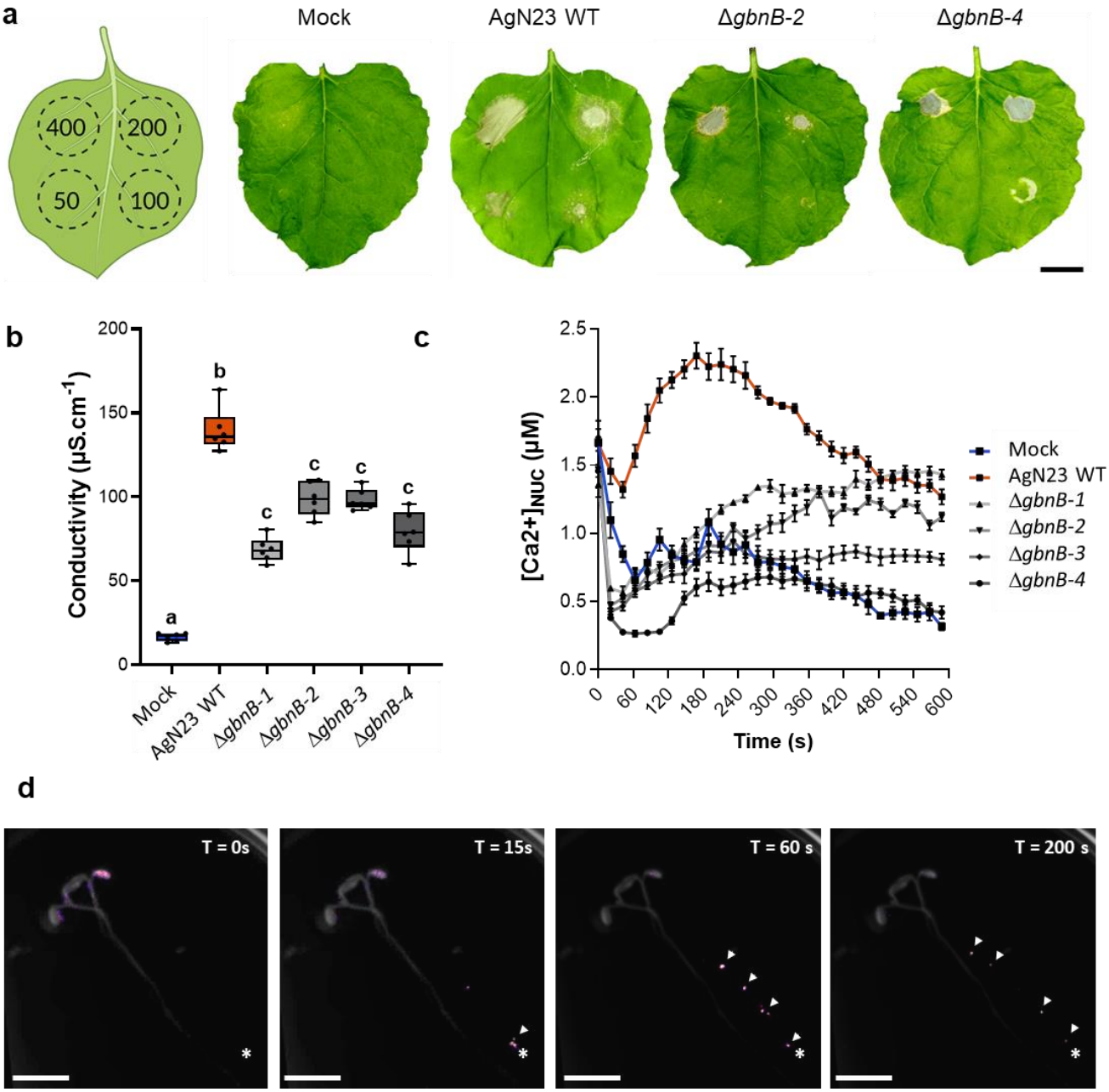

Figure 5: **The Culture Media Extract of AgN23 triggers a galbonolides dependent hypersensitive response a.** Typical photographs of necrotic symptoms in *Nicotiana benthamiana* leaves 48h after infiltration with CME of AgN23 WT or KO mutants (Δ*gbnB-2* and Δ*gbnB-4*) at 50, 100, 200 and 400 µg/mL as indicated in the scheme (n = 6). Scale bar: 3 cm. **b.** Ion leakage measurements of *Arabidopsis* leaf disks infiltrated with CME of AgN23 WT or KO mutants (Δ*gbnB*) at 100 µg/mL. Box plots were created with data from 6 independent assays involving 5 to 6 leaf disks (n = 6). The letters a–c indicate statistically significant differences according to one-way analysis of variance (ANOVA) and Tukey's HSD test (Honestly Significantly Different, α = 0.05). **c.** Kinetics of AgN23 or KO mutants CME-induced nuclear calcium influxes in *Arabidopsis seedlings expressing* nuclear-localized aequorin. CME at 100 µg/mL was added at time = 0 min. Graphs show the mean ± SD calculated from 10 independent assays involving 3 plants per treatment (n = 10). **d.** EM-CCD observations of calcium waves in the nuclei of an aequorin-expressing *Arabidopsis* seedling. Plants were inoculated at the root apex (white asterisk) with CME of AgN23 WT at 100 µg/mL. White arrows show luminescent nuclei (n = 3). Scale bar: 2 cm.

324

325 To investigate the impact of galbonolides production on root development, *in vitro* grown seedlings
326 were inoculated with galbonolides mutants. As shown on figure 6a and 6b, no root growth inhibition
327 was observed with the two mutants. Furthermore, we noted that the robust induction of expression
328 in *PR1*, *PAD3,* and *PAD4* by AgN23 CME was compromised when using the 4 galbonolides KO mutants
329 (Figure 6c). Thus, our data prove that galbonolides are required for the activation of immune gene
330 expression in *Arabidopsis* seedlings in response to AgN23.

331 In view of our finding that *Arabidopsis* responds to AgN23 by strongly activating camalexin
332 biosynthesis, we studied the effect of *in vitro* spore inoculation of Col-0 with AgN23 and the two
333 galbonolide mutants Δ*gbnB-2* and Δ*gbnB-4*, by LC-HRMS metabolic fingerprinting (Data S4). The PCA
334 revealed a significant difference in the metabolome response to the two AgN23 mutants as compared
335 to the wild type (Figure 6d). Strikingly, the induction of camalexin detection was significantly lower in
336 roots inoculated with galbonolides mutants as compared to the wild type bacterium (Figure 6e).

337 Soil inoculation with galbonolides mutants did not produce a dwarf phenotype triggered by AgN23
338 on Col-0 rosette (Figure 6f, 6g). Lastly, we analysed the colonisation of Col-0 rhizosphere by wild type
339 and galbonolide mutants AgN23 and we did not observe an enrichment of the galbonolides mutants
340 in the rhizosphere (Figure 6h). Put together, these data clearly point to the crucial role played by
341 galbonolides for the induction of plant responses as well as the rhizospheric fitness of the bacterium.

342

343

344

345

346

347

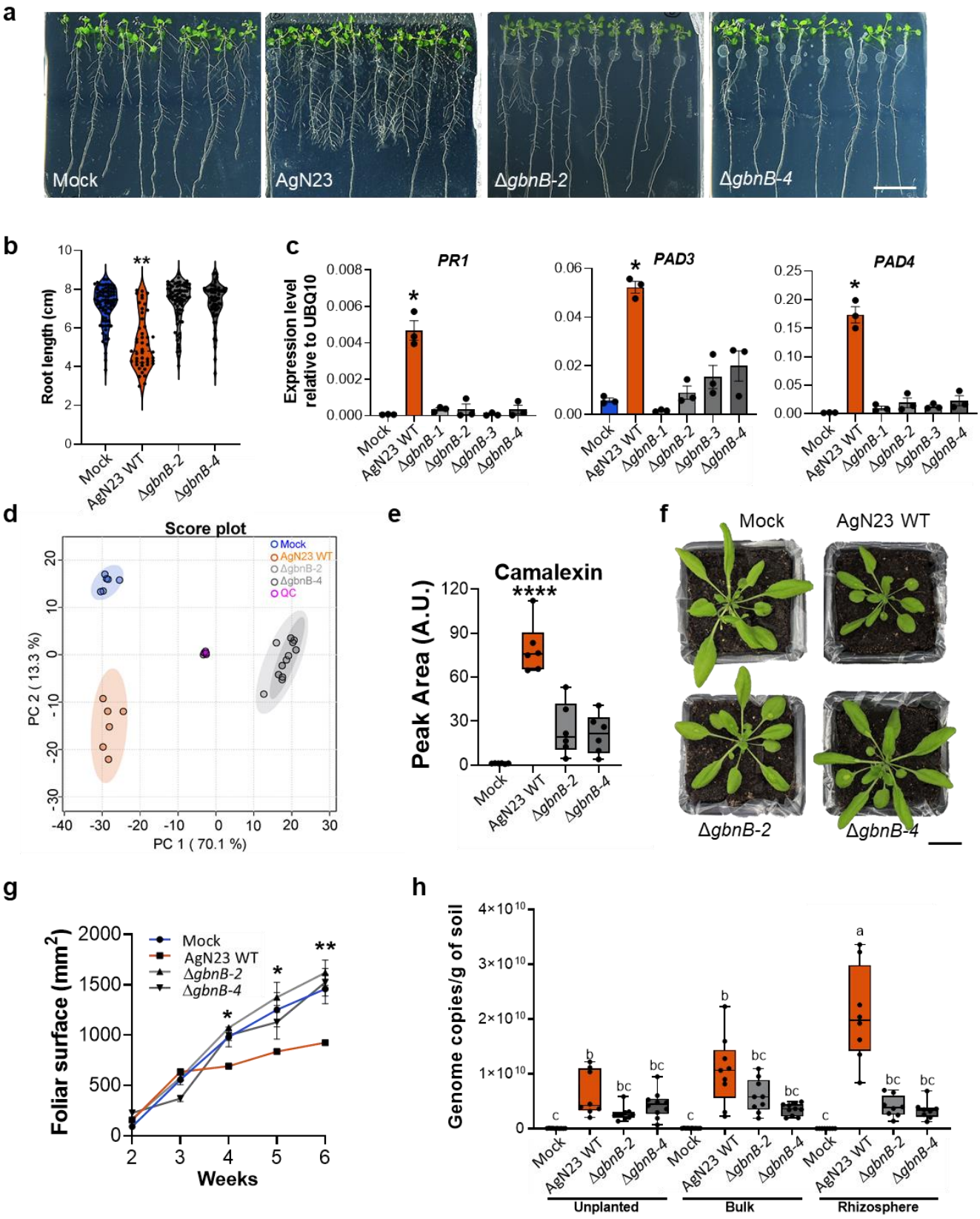
a
Mock
AgN23
ΔgbnB-2
ΔgbnB-4
b
Root length (cm)
Mock
AgN23 WT
ΔgbnB-2
ΔgbnB-4
c
Expression level relative to UBQ10
PR1
PAD3
PAD4
Mock
AgN23 WT
ΔgbnB-1
ΔgbnB-2
ΔgbnB-3
ΔgbnB-4
d
Score plot
Mock
AgN23 WT
ΔgbnB-2
ΔgbnB-4
QC
PC 1 (70.1 %)
PC 2 (13.3 %)
e
Camalexin
Peak Area (A.U.)
f
Mock
AgN23 WT
ΔgbnB-2
ΔgbnB-4
g
Foliar surface (mm²)
Weeks
Mock
AgN23 WT
ΔgbnB-2
ΔgbnB-4
h
Genome copies/g of soil
Unplanted
Bulk
Rhizosphere

348

349 **Figure 6: Galbonolides play a crucial role in defense gene activation, camalexin biosynthesis and**
350 **AgN23 persistence in the rhizosphere**. **a.** Observation of *Arabidopsis thaliana* Col-0 colonization by
351 AgN23 WT or KO mutants at 10 days after inoculation with spores at the root apex. Scale bar: 2 cm. **b.**
352 Primary root length of plants colonized by AgN23 WT or KO mutants (Δ*gbnB*) at 10 days after
353 inoculation. Statistical differences between the treatments were analyzed using Mann–Whitney test
354 and '****' represents significant differences at $p < 0.0001$. **c.** Analysis of *PR1*, *PAD3*, and *PAD4* defense
355 gene expression in 10-day old *Arabidopsis* seedlings at 6 hours after treatment with AgN23 CME.
356 Graphs show the mean $2^{-\Delta Cp}$ relative to *UBQ10* and SD calculated from three biological replicates (n =
357 3), each involving five plants. Statistical comparisons were performed with T-test ('*' = $p < 0.05$). **d.**
358 PCA score plot of UHPLC-HRMS data (n = 256 variables) from extracts of *Arabidopsis thaliana* 10 days
359 after inoculation with AgN23 WT or KO mutants (Δ*gbnB*) **E.** Average peak area of camalexin. Box plots
360 were created from data from six independent assays (n = 6). The whiskers encompass the minimum
361 and maximum values, and the midline shows the median. Statistical differences between the
362 treatments were analyzed using unpaired T-test and '****' represents significant differences at p <
363 0.0001.**f.** Typical photographs of 6-week-old Col-0 rosettes grown in potting soil inoculated with
364 AgN23 WT or KO mutants spores. Scale bar: 1.7 cm **g.** Leaf area measurement. Graphs show the mean
365 ± SD calculated from at least eight biological replicates (n = 8). **h.** AgN23 WT and Δ*gbnB-2* and Δ*gbnB-*
366 *4)* mutants genome copy number in Col-0 rhizosphere 6 weeks after soil inoculation. Box plots were
367 created from data from 8 plants per treatment (n = 8). The whiskers encompass the minimum and
368 maximum values, and the midline shows the median. The letters a–c represent statistical differences
369 between the treatments based on 2-way ANOVA followed by Tukey's multiple comparisons test.

370

371 **DISCUSSION**

372 Understanding chemical basis of the communication which established between plants and associated
373 microorganisms is essential to improve the function and composition of plant microbiota, notably in
374 the context of developing sustainable agriculture practices. Towards this effort, *Streptomyces* species
375 could play a major role due to their ability to efficiently colonize the rhizospheric niche and to produce
376 a wide array of specialized metabolites with various biological activity. However, mechanisms involved
377 in the establishment and long-term maintenance of active microbial strains in the rhizosphere are
378 largely unknown. In this study, we identify how a *Streptomyces* strain, AgN23, promotes its
379 development in the rhizosphere through the production of a metabolite which triggers the plant's
380 production of an antimicrobial compound.

381 AgN23 is a strain that was initially isolated from the rhizosphere of grape and belongs to the *S.*
382 *violaceusniger* clade including species found in various environments and notably, in the rhizosphere.
383 Here, we show that AgN23 efficiently colonizes the rhizosphere of *A. thaliana* and that this

384 colonization negatively impacts the growth of the plant. Taking a cue from our previous work where
385 we showed that AgN23 induced strong defence responses when applied on foliar tissues, we
386 hypothesized that its effect on plant growth could be due to a trade-off between the induction of
387 defence and plant growth, a commonly observed tendency in plants[27,42]. Accordingly, we carried out
388 metabolic fingerprinting of *Arabidopsis* response to AgN23 which showed that plant response is
389 mainly characterized by the production of camalexin, a well-known phytoalexin produced by *A.*
390 *thaliana*[43]. Next, we used the *pad3-1* camalexin deficient mutant of *Arabidopsis* to demonstrate that
391 the efficient colonization of the rhizosphere by AgN23 relied on the production of this compound by
392 the plant. Interestingly, *pad3-1* did not show symptoms or signs of over colonisation by AgN23,
393 suggesting that camalexin does not act as an inhibitor of AgN23. Thus, the precise role of camalexin in
394 supporting the development of AgN23 in the rhizosphere remains to be elucidated, but it can be
395 hypothesized that the induction of camalexin can reduce the proliferation of susceptible bacteria and
396 fungi and thereby facilitate colonization of the rhizosphere by AgN23[44]. Rhizosphere colonisation by
397 microorganisms relies on their ability to exploit exudates released by the plant[45]. Microorganisms can
398 also provoke plant defence activation by triggering various kinds of responses, such as induced
399 systemic resistance (ISR)[46]. The recent discovery that mutations in plant immunity and hormonal
400 signalling pathways led to an alteration in root microbiota serves to further highlight the pivotal role
401 of host defence responses in the root microbiota recruitment process[47-50]. For example, *Arabidopsis*
402 root inoculation with the proteobacteria *Pseudomonas simiae* WCS417 results in the secretion of
403 scopoletin, a coumarin that facilitates *P. simiae* root colonisation while inhibiting the growth of fungal
404 pathogens and diverse other bacterial taxa[46]. Similarly, the Plant Growth Promoting Rhizobacteria
405 (PGPR) *Pseudomonas* sp. CH267 triggers the production of the indole alkaloid camalexin, which
406 incidentally, is the primary *Arabidopsis* phytoalexin involved in the regulation of root microbiota
407 composition and the recruitment of PGPRs[51,52]. Similarly to the aforementioned strains, we propose
408 AgN23 behave as a PGPR in the rhizosphere.To understand the molecular mechanisms underlying the
409 induction of plant defence by AgN23, we investigated the composition of the bacteria exometabolome

410 using untargeted metabolomic tools. This analysis revealed several specialised compounds with
411 known antimicrobial activity, and for some of them, a putative function in eliciting plant defences was
412 seen. Among these compounds, we decided to delve into the role of galbonolides in AgN23's biological
413 activities on plants, since it has been shown that galbonolides targeted the sphingolipid metabolism,
414 which is known to play a major role in plant defence signalling[53]. Moreover, the specific activation of
415 camalexin in response to AgN23 is a typical response of sphingolipid signalling[33]. Disrupting the
416 galbonolide gene cluster resulted in the mutants lacking the production of all the galbonolide-derived
417 products. This is in line with previous findings indicating that all galbonolide variants are produced
418 through a single BGC[54-57]. The structure and bioactivities of galbonolides from *Micromonospora*
419 *narashinoensis* (initially named rustmicin) and *Streptomyces* galbus have been elucidated nearly 40
420 years ago [39,58-63]. Follow up studies have shown that these compounds act by inhibiting the IPC
421 synthase in both plants and fungi [64]. Galbonolides have therefore been investigated mainly for their
422 antifungal properties and their effects on plants have not been thoroughly characterised. Inositol
423 Phosphorylceramide Synthase are involved in plant sphingolipid metabolism and we postulate that
424 IPCS inhibition by AgN23 may result in locally modifying the ceramide composition. As exemplified by
425 Fumonisin B1 produced by pathogenic *Fusarium* sp., the disturbance of the sphingolipid homeostasis
426 is a trigger for SA signalling and hypersensitive response, resulting in disease development[65,66].

427 To investigate the role of galbonolides in the induction of plant defences by AgN23, we performed
428 a set of complementary experiments based on calcium signalling, plant gene expression and plant
429 metabolomics studies, results of which, all pointed to the requirement of galbonolides to trigger plant
430 responses to AgN23 colonization. While it cannot be excluded that other AgN23 compounds are able
431 to induce some defence reactions, our results demonstrated that galbonolides are the major
432 components of the eliciting activity of AgN23 and notably, the strong HR-like symptoms and the
433 stunted phenotype. Finally, the lack of enrichment of AgN23 galbonolide mutants in the *Arabidopsis*
434 rhizosphere show that these induction of plant defence, and notably the production of camalexin, by
435 these compounds are beneficial for the AgN23 rhizospheric lifestyle (Figure 7).

436 In this study, we combined genetic and metabolomic approaches both on *Streptomyes* sp. AgN23
437 and the host plant *Arabidopsis* to discover a new ecological function for galbonolides. We unravelled,
438 for the first time, how galbonolides allow an actinobacteria to better thrive in the plant rhizosphere.
439 The recent functional validation of gene clusters involved in galbonolides biosynthesis allowed us to
440 confirm by genome mining, the widespread potential of rhizosphere *Streptomyces* and *Actinobacteria*
441 to produce them [28,40,54]. Since the galbonolide target, the IPCS, is ubiquitous among plant species, we
442 propose that the role of galbonolides can be generalized in cross-kingdom communication between
443 plant and actinomycetes[67]. The precise impact of galbonolides on surrounding microbes within the
444 rhizosphere has still to be addressed to provide a comprehensive understanding of galbonolides' roles
445 in the plant environment.

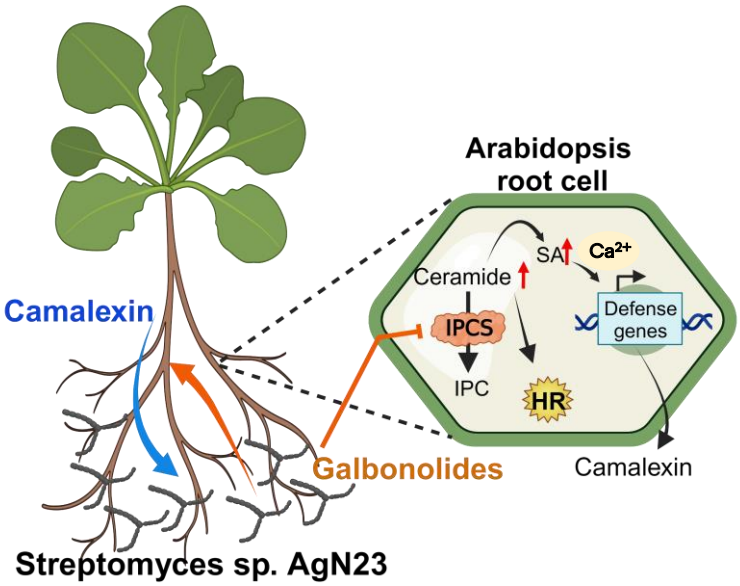

446

447 **Figure 7: Model summarizing the mode of action of galbonolides in stimulating plant defence to**
448 **support AgN23 colonization of the rhizosphere.** Galbonolides secretion by *Streptomyces* sp. AgN23
449 trigger Inositol Phosphoceramide Synthase (IPCS) inhibition in *Arabidopsis* root cells (orange arrow).
450 The resulting raise in Ceramide precursors of the IPCS may result in the different defence responses
451 associated to AgN23: Hypersensitive Responses (HR), Salicylic Acid (SA) signalling, nuclear Ca^{2+} influx,
452 defence gene expression and camalexin biosynthesis. This production of camalexin (blue arrow) exert
453 a positive effect on AgN23 growth in the rhizosphere, presumably by restricting the growth of bacterial
454 and fungal competitors sensitive to this phytoalexin. In addition, galbonolides secretion in the
455 rhizosphere may also directly interfere with fungal competitors of AgN23.

ACKNOWLEDGEMENTS

We thank Dr. Paul Denny (Warwick University) for sharing the yeast line that allowed to purify microsomal fractions bearing *AtIPCS2,* and Dr. Pawel Bednarek for the *pad3-1* seeds.

AUTHOR CONTRIBUTIONS

Clément Nicolle, Damien Gayrard, Alba Noël, Marion Hortala, Guillaume Marti, Aurélien Amiel, Sabine Grat-Simeone and Aurélie Le Ru performed the research. Clément Nicolle, Jean-Luc Pernodet, Sylvie Lautru, Bernard Dumas and Thomas Rey wrote the paper.

DECLARATION OF INTERESTS

The following information may be seen as competing interests. B.D. is one of the inventors of the patent WO2015044585A1 related to the use of AgN23 in agriculture. T.R. and D.G. are full-time researchers at the AgChem company De Sangosse (Pont-Du-Casse, France), which registers and markets crop-protection products and owns the patent WO2015044585A1.

FUNDING

This work was funded by the Fond Unique Interministériels (NEOPROTEC project), the Fonds Européen de Développement Économique et Régional (FEDER), the Agence Nationale de la Recherche (LabCom BioPlantProtec ANR-14-LAB7-0001 and STREPTOCONTROL ANR-17-CE20-0030), and the Région Occitanie (projet GRAINE-BioPlantProducts). The Laboratoire de Recherche en Sciences Végétales (LRSV) belongs to the TULIP Laboratoire d'Excellence (ANR-10-LABX-41) and benefits from the “École Universitaire de Recherche (EUR)” TULIP-GS (ANR-18-EURE-0019). Work performed in the GeT core facility, Toulouse, France (https://get.genotoul.fr) was supported by the France Génomique National infrastructure, funded as part of the “Investissement d'Avenir” program managed by the Agence Nationale de la Recherche (contract ANR-10-INBS-09) and by the GET-PACBIO program (FEDER Programme opérationnel FEDER-FSE MIDI-PYRENEES ET GARONNE 2014-2020). D. Gayrard was funded by the Agence Nationale de la Recherche Technique, with the « Convention Industrielle de

480 Formation par la Recherche and Association Nationale de la Recherche et de la Technologie » (Grant
481 N° 2016/1297). C. Nicolle was funded by the Ministère de l'Enseignement Supérieur et de la Recherche
482 (PhD fellowship)

483 **DATA AVAILIBILITY**

484 Datasets generated or analyzed during this study are included in this published article (and its
485 Supplementary Dataset files). Raw data regarding RNAseq analysis can be found on the NCBI Gene
486 Expression Omnibus (GSE119986) and their complete analysis can be found in Vergnes et al., 2019.
487 The genome assembly of AgN23 is available on the NCBI "Nucleotide" repository (NZ_CP007153.1)
488 with the chromosome sequence and the automatic annotation pipeline used to define gene models
489 in this study; a detailed analysis of the genome is available in Gayrard et al., 2023. The LC-HRMS
490 chromatograms of AgN23 CME and *Arabidopsis* are available on Zenodo repository (8421008).

491 **METHODS**

492 **Plant material and growth conditions, and phenotyping**

493 Seeds of *Arabidopsis thaliana* accession Col-0 (N1092) were obtained from the Nottingham
494 Arabidopsis stock center (NASC) and mutant *pad3-1* (N3805) were kindly provided by Dr. Pawel
495 Bednarek. *Arabidopsis* plants grown in potting soil (PROVEEN; Bas Van Buuren B.V., Holland) were
496 cultivated in a growth chamber under 16 h photoperiod and 23 °C unless otherwise indicated. Similar
497 conditions were applied to the cultivation of *Nicotiana benthamiana*. One-month-old *N. benthamiana*
498 leaves were syringe-infiltered with bacterial CMEs. Cell death areas were photographed 24–48h after
499 infiltration, with an Expression 11000 XL scanner (Epson) at 300 dots/inch.

500 For *in vitro* cultivation, seeds of *Arabidopsis* were surface sterilized with a mixture containing 25%
501 NaClO and absolute ethanol in the volume ratio 1:5 for 10 min and then rinsed two times with 95%
502 ethanol. Ethanol was discarded and the seeds were allowed to dry completely. Seeds were then sown
503 onto Murashige and Skoog (MS, Sigma) at 4.4 g/L supplemented with agarose (Sigma) 8 g/L and

504 adjusted to pH 5.7. Surface sterilized seeds were allowed to sprout in a growth phytotronic chamber
505 (16 h photoperiod, 23°C) on vertically placed plates filled with MS medium amended with 1 % sucrose.
506 2 days after germination, seedlings were transferred to 12 cm^2 square Petri dishes containing 1x
507 sucrose-free MS medium at the rate of 10 seedlings per dish. Four-day old seedlings were then
508 inoculated at the root tip with 10 µL of spore inoculum at 10^5 CFU/mL and placed back vertically in the
509 growth phytotronic chamber. 10 µL of sterilized ultrapure water was used for mock treatments. Root
510 phenotype was observed 10 days after inoculation and photographs were taken with an Expression
511 11000 XL scanner (Epson) at 300 dots/inch. Primary root lengths were measured with Image J software
512 (v. 1.51k).

513 To perform nuclear calcium influx studies, we used an *Arabidopsis* transgenic line expressing the
514 chimeric construct containing the 35S promoter controlling the nucleoplasmin coding region in frame
515 with the coding region of apo-Aequorin as described previously [68]. The vector was transformed into
516 the *Agrobacterium tumefaciens* LBA4404 strain and Col-0 transgenic plants carrying the 35S::apo-
517 aequorin-nuc were generated using the floral dip method and selected in 50 µg/mL hygromycin B[69].
518 Surface sterilized *Arabidopsis thaliana* 35s::apo-aequorin-nuc were cultivated on vertically placed
519 plates filled with ½ MS medium amended with 1% sucrose and with a sterile 120 × 120 mm Nytex
520 fabric (mesh opening 37 µm; Sefar) layered on top. Three 10-day old seedlings were sampled and
521 placed in 11 x 55 mm 3 mL polystyrene tubes and considered as one replicate. For gene expression
522 assays, Col-0 seeds were surface sterilized and transferred into the wells of 24-well plates containing
523 300 µL ½ MS + 1% sucrose medium. Seeds were allowed to sprout in a growth chamber (16 h
524 photoperiod, 23°C) mounted on a rotary shaker at 90 rpm for 2 days. 5 seedlings per well were kept
525 and the plates were transferred on a static tray. ½ MS + 1% sucrose medium was replaced with 300
526 µL of fresh medium 7 days after germination. The seedlings were then treated with 300 µL of CME at
527 200 µg dry extract/mL added to each well 10 days after germination. Sampling was performed at 1, 6,
528 and 24 h after treatment, the seedlings being immediately thrown into liquid nitrogen and stored at -
529 80 °C until RNA extraction.

530 To perform soil inoculation assays with AgN23, 70 g of potting soil inoculated with AgN23 spore
531 inoculum at 10^4 CFU/g was distributed in pots placed in small plastic bags to avoid cross-contamination
532 during watering. 5 to 10 *Arabidopsis* seeds were sown per pot and the pots were placed in a growth
533 phytotronic chamber. A single seedling was kept per pot 5 days after germination. Pots were watered
534 weekly with 10 mL of tap water. The watering pots were photographed to monitor the aerial part
535 phenotype. Green area was measured with ImageJ (v. 1.51k) at 4, 6 or 7 weeks after inoculation.

536 **AgN23 cultivation and transgenesis**

537 AgN23 strain was cultivated on the solid medium Soya Flour Mannitol (SFM) medium (D-Mannitol
538 (Sigma) 20 g/L; organic soya flour (Priméal) 20 g/L; Bacto™ Agar (Difco Laboratories) 20 g/L) for the
539 purpose of spore production and genetic manipulations.

540 To produce spore inoculum, SFM plates were incubated for two weeks at 28°C in darkness before
541 filling them with 10 ml of sterile ultrapure water. The mycelium was thoroughly scraped with a sterile
542 spreader and the resulting solution was vortexed, then filtered in a 20 ml syringe filled with sterile
543 cotton wool. The resulting suspension was centrifuged at 4,200 rpm for 10 min. The supernatant was
544 discarded, the pellet re-suspended in sterile ultrapure water, and the resulting suspension was
545 adjusted to 10^5 CFU/mL.

546 AgN23 was grown in Bennett medium for the purpose of liquid state cultivation and of CME
547 (Culture Media Extract) (D-Glucose 10 g/L; Soybean peptones 2.5 g/L; Yeast Extract 1.5 g/L; Sigma).
548 The culture was set in 250 mL Erlenmeyer flasks by inoculating 50 mL Bennett medium with 100 µL of
549 fresh spore suspension at 10^5 CFU/mL at 250 rpm and 28 °C in a shaking incubator at 250 rpm for 7
550 days.

551 *Escherichia coli* strains were grown in LB with appropriate antibiotics as necessary. *E. coli*
552 transformation and *E. coli* / *Streptomyces* conjugation were performed according to standard
553 procedures. Phusion High-fidelity DNA Polymerase (Thermo Fisher Scientific) was used to amplify DNA
554 fragment except for PCR verification of plasmids or strains for which Taq polymerase (Qiagen) was

555 used. DNA fragments and PCR products were purified using the Nucleospin Gel and PCR clean up kit
556 (Macherey-Nagel). All oligonucleotides used in this work were purchased from Integrated DNA
557 Technologies(Data S5).

558 For pOSV700 plasmid construction, a 0.4 kb DNA fragment encompassing the ermEp* promoter
559 and the tipA ribosome binding site (RBS) was amplified from pOSV666 using the primers JWseq6 and
560 JWseq7 . The fragment was digested by EcoRV and cloned into EcoRV-digested pSET152, resulting in
561 pOSV700. The sequence of the insert was verified.

562 For GFP and mCherry transgenesis, the sequences of the soluble-modified GFP (smGFP) and
563 mCHERRY genes were optimized for expression in Streptomyces, synthesized as gblocks (IDT) and
564 cloned into pGEM-T easy, resulting in pmsolGFP and pmCHERRY, respectively. The smGFP and
565 mCHERRY genes were amplified from these plasmids using the primer pairs onSC001/onSC011 and
566 onSC005/onSC013, respectively. PCR amplicons were digested by NdeI and PacI and cloned into
567 NdeI/PacI-digested pOSV700. The resulting plasmids were verified by restriction digestion and
568 sequencing, and named pSC001 (smGFP) and pSC003 (mCHERRY). These were subsequently
569 introduced in E. coli ET12567/pUZ8002 and transferred into Streptomyces sp. AgN23 by intergeneric
570 conjugation. Conjugants were selected on apramycin 50 µg/ml. The resulting strains were verified by
571 PCR on the extracted genomic DNA using the pSET152-F and pSET152-R primers.

572 For production of galbonolides knock-out mutants, a 5 kb internal fragment of *gbnB* coding for the
573 structural PKS gene of the galbonolides biosynthetic gene cluster was replaced by a kanamycin
574 resistance cassette. For this purpose, a 2kb fragment (upstream fragment) encompassing the
575 beginning of *gbnB* was amplified by PCR with the onSC007/onSC008 primer pair and cloned into
576 pGEM-T Easy, yielding pSC008. Similarly, a 2kb fragment (downstream fragment) encompassing the
577 end of *gbnB* was amplified by PCR with the onSC009/onSC010 primer pair and cloned into pGEM-T
578 Easy, yielding pSC009. The pSC008 and pSC009 plasmids were digested by EcoRI/EcoRV and
579 DraI/HindIII, respectively, and the 2 kb fragments (upstream and downstream fragments respectively)

580 were purified on agarose gel. The kanamycin resistance cassette was obtained by digesting pOSV514
581 by EcoRV. The three fragments (upstream, downstream and resistance cassette) were next ligated
582 into EcoRI/HindIII-digested pOJ260. The resulting plasmid, named pSC004, was verified by digestion
583 with BamHI, PstI, EcoRI and EcoRV. Five independent conjugants were verified by PCR using the
584 onSC022/onSC023, onSC021/JWseq16, and onSC030/JWseq17 primer pairs.

585 **Analysis of *Arabidopsis* defence response**

586 The loss of electrolytes from dying cells due to hypersensitive response related programmed cell death
587 (HR-PCD) was monitored according to a vacuum-based infiltration method of leaf material as
588 described previously[70]. Briefly, *Arabidopsis* leaf discs, prepared with a cork borer (5 mm diameter),
589 were covered in 10 mL of bacterial culture supernatant extract at 100 µg dry extract/mL and placed in
590 a SpeedVac vacuum concentrator (Thermo Scientific™). After infiltration, the discs were poured into
591 a tea strainer, rinsed with ultrapure water, and transferred to 6-well cell cultivation plates filled with
592 10 mL ultrapure water (4–5 discs in each well in 6 replicates per treatment). Conductivity was
593 measured by transferring 8 mL of the bathing solution to a 15 mL centrifuge tube in which an InLab
594 731-ISM conductivity cell (Mettler Toledo) was placed. The solution was returned to the plate well
595 after measurement. Plates were kept in a growth phytotronic chamber (16 h photoperiod, 23°C)
596 between measurements.

597 Ca^{2+} signals in the nuclei of *Arabidopsis thaliana* cells were quantitatively measured as described
598 previously[71]. Holoaequorin was reconstituted by adding 400 µL of 2.5 µM coelenterazine (Interchim)
599 solution to the tube followed by overnight incubation in darkness. At time 0, the coelenterazine
600 solution was removed and the tube was placed in a Sirius single tube luminometer (Berthold
601 Technologies). A volume of 400 µL of AgN23 WT or AgN23 KO mutants supernatant culture extracts
602 at 100 µg dry extract/mL were then gently added on the seedlings and photon counting was
603 immediately started by closing the luminometer chamber. After the Ca^{2+} response reached the initial
604 baseline level, 300 µL of lysis solution (100 mM $CaCl_2$ in 10% ethanol supplemented with 2% Nonidet
605 P40 (v/v)) were automatically injected in the polypropylene tube to discharge the free aequorin owing

606 to the calcium-enriched medium. The emitted light was calibrated in terms of Ca^{2+} concentrations

607 using a previously described method[72].

608 $$[Ca^{2+}] = \frac{(\frac{L_0}{L_{max}})^{1/3} + \left[KTR \times \left(\frac{L_0}{L_{max}}\right)^{\frac{1}{3}}\right] - 1}{KR \times \left(\frac{L_0}{L_{max}}\right)^{\frac{1}{3}}}$$

609 L_0 is the luminescence intensity/s and L_{max} is the total amount of luminescence present in the entire

610 sample over the course of the experiment. [Ca2+] is the calculated Ca^{2+} concentration, KR is the

611 dissociation constant for the first Ca^{2+} ion to bind, and KTR is the binding constant of the second Ca^{2+}

612 ion to bind to aequorin. The luminescence data were determined using the KR and KTR values of 7 ×

613 10^6 M^{-1} and 118, respectively. For time course imaging, 5-day old *Arabidopsis thaliana* 35s::Aequorin-

614 nuc seedlings were placed in 60 mm petri dishes filled with ½ MS medium. Holoaequorin was

615 reconstituted by adding 500 µL of 2.5 µM coelenterazine (Interchim) solution to the dish followed by

616 overnight incubation in darkness. At time 0, the coelenterazine solution was removed and plants were

617 treated by adding 10 µL of supernatant culture extracts at 100 µg dry extract/mL at the root apex.

618 Images were acquired with a homemade system based on a EM-CCD camera (C9100-13, Hamamatsu)

619 driven by HC-image software (Hamamatsu) and a macro objective. Both system and sample were

620 placed in a dark room during the experiment. The camera was set to EM-CCD mode with the gain set

621 at 5 and 1200, and the exposure time was 5 s. Images were analysed with the ImageJ software package

622 (http://rsb.info.nih.gov/ij/; v. 1.51k)

623 For defence gene expression assays, total RNAs were extracted using the RNeasy Plant Mini Kit

624 (Qiagen) and DNase treated with RQ1 RNase-Free DNase (Promega). For each sample, 1 µg of total

625 RNA was reverse-transcripted with the High Capacity cDNA Reverse Transcription Kit (Applied

626 Biosystems). cDNAs were diluted to 1 ng/ µL and used for qPCR analysis in a 10 µL reaction mix

627 containing 5 µL of LightCycler® 480 SYBR Green I Master mix (Roche), 300 nM of each primer, and 2

628 µL of the diluted template cDNAs. qPCR was performed in triplicate using a LightCycler ® 480 System

629 (Roche) with preheating at 95 °C for 5 min and then 40 cycles of 95 °C for 15 s and 60 °C for 60 s. The
630 Polyubiquitin 10 gene AT4G05320 was retained for normalization. The $2^{-\Delta Cp}$ method was used to
631 display gene expression levels [82]. Primers used in this study are listed in Data S5.

632 **AgN23 DNA quantification from soil and rhizosphere DNA**

633 To track the development of AgN23, the plants were removed from the soil. The remaining soil from
634 each pot was homogenized and a small amount was sampled and considered as bulk sample. Roots
635 were placed into 50 mL conical sterile polypropylene centrifuge tubes filled with 20 mL 1X phosphate-
636 buffered saline (pH 7.4), and vigorously vortexed to release the adhering rhizospheric soil. Tubes were
637 then centrifuged at 4000 rpm and the washing step was repeated one time. Soil pellets after second
638 centrifugation step were considered as rhizosphere samples. Samples were stored at -80°C until
639 processing. The total microbe DNA from 100 mg of bulk or rhizosphere samples was extracted using
640 the *Quick*-DNA™ Fecal/Soil Microbe Miniprep kit (Zymo Research) following manufacturer's
641 instructions. DNA was eluted in 100 µL DNA Elution Buffer and quantified with DS-11
642 Spectrophotometer/Fluorometer (DeNovix) and stored at -80°C until processing.

643 AgN23 specific primers were designed to quantify the AgN23 genome copy number by qPCR
644 analysis. Briefly, 10 kilobases portions of the AgN23 genome gapless assembly (GCF_001598115.1)
645 was blasted with NCBI Primer-BLAST with default settings except for PCR product size (70-200 bp),
646 database (nr) and organism (Streptomyces taxid:1883). Primers AgN23-F (5'-
647 CATGGGTTTCTGTGGCCTCT-3') and AgN23-R (5'-AGATGGTTCACGCCCACATT-3') were found and
648 validated experimentally to target a unique intergenic region (2108022-2108187) and resulted in a
649 166-bp long PCR product with Tm = 59.96 °C (Data S5). qPCR was performed in triplicate using a CFX
650 Opus Real-Time PCR System (Biorad). Each qPCR reaction was performed in 10 µL with the LightCycler®
651 480 SYBR Green I Master mix (Roche), 300 nM of each primer, and the template DNA. 4 ng of total
652 DNA extracted from soil samples was used. The amplification conditions were as follows: preheating
653 at 95 °C for 5 min followed by 40 cycles of 95 °C for 15 s and 60 °C for 60 s. Melting curves were

654 checked to confirm purity of the amplified product. AgN23 pure genomic DNA was isolated as
655 described previously [28], quantified, and serial dilutions were performed to determine AgN23 genome
656 concentration in soil samples. The number of gene copies per g of soil (N) was calculated as:

657 $$m_{AgN23} = \frac{S_{AgN23} \times M_{bp}}{Na}$$

658 $$N = \frac{D_{well} \times C_{sample} \times 50{,}000}{m_{AgN23}}$$

659 Where m_{AgN23} is the mass of one genome copy of AgN23 in ng ($1.08.10^{-5}$ ng), S_{AgN23} is AgN23 genome
660 length in base (S_{AgN23} = 10.9 Mb), M_{bp} is the molecular mass of one base pair (600 g/mol), Na the
661 Avogadro constant (Na = $6.022.10^{23}$ mol^{-1}), D_{well} is the DNA mass calculated in a well of qPCR reaction
662 in ng, and C_{sample} is the total DNA concentration of 100 mg of soil sample in ng/µL.

663

664 **Preparation of samples for biochemistry studies**

665 For root metabolome studies, 10 *Arabidopsis* seedlings from the same MS plate were sampled
666 together in 2 mL microtubes containing two 3 mm-diameter tungsten carbide beads (Qiagen), and
667 flash frozen in liquid nitrogen. Samples were ground 2 times *via* bead beating with a mixer mill (Retsch)
668 at 30 Hz for 30 s. 100 mg of plant powder were placed into lysing matrix D 2 mL tubes (MP Biomedicals)
669 containing 1 mL of extraction buffer (CH_3OH: C_3H_8O: H_2O: CH_2O_2 = 40: 40: 19.5: 0.5) ground twice for
670 20 s with a FastPrep-24™ homogenizer (MP Biomedicals) at 6.5 m/s. Samples were re-frozen in liquid
671 nitrogen between each cycle. The supernatants were isolated by centrifugation at 10,000 g for 20 min
672 and concentrated in a Speedvac vacuum concentrator (Thermo Scientific™). Samples were then
673 resuspended in 1 mL of injection buffer (50 % CH_3OH 50% H_2O) and filtrated through 750µL nonsterile
674 micro-centrifugal filters (PTFE; 0.2 µm; Thermo Scientific) and introduced in HPLC certified vials. An
675 aliquot of each sample from the same extraction series was pooled together for quality control (QC).

676 For studies of AgN23 culture media extract (CME), the bacterial biomass grown in liquid flask
677 culture was removed from the culture supernatant by centrifugation at 4,200 rpm for 10 min,

678 completely dried in oven at 50 °C, and weighed to assess AgN23 growth. To pull out specialized
679 metabolites from the CME, 60 g/L of amberlite XAD-16 (Sigma) was added to each culture flask
680 supernatant and mixed overnight at 250 rpm and 28 °C in a shaking incubator. Subsequently, XAD-16
681 was separated through vacuum filtration and the liquid was discarded. The separated XAD-16 was
682 then placed in 50 mL butanol for 4 h and flasks were regularly hand-shaken. One more vacuum
683 filtration was then carried out, the XAD-16 was discarded, and the resulting butanol extracts were
684 then concentrated by rotary evaporation with a Rotavapor® R-300 (Buchi). The concentrated extracts
685 were placed in calibrated 5 mL test tubes, completely dried under nitrogen flow, weighed, and
686 adjusted to 2 mg/mL in 50% CH_3CN 50% H_2O mixture. Finally, 700 µL quantities of the diluted extract
687 were filtrated through 750µL nonsterile micro-centrifugal filters (PTFE; 0.2 µm; Thermo Scientific) and
688 introduced in HPLC certified vials. An aliquot of each sample from the same extraction series was
689 pooled together for quality control (QC).

690 **UHPLC-HRMS profiling, feature annotations and statistical analysis**

691 Ultra-High-Performance Liquid Chromatography-High Resolution MS (UHPLC-HRMS) analyses were
692 performed on a Q Exactive Plus quadrupole mass spectrometer equipped with a heated electrospray
693 probe (HESI II) coupled to a U-HPLC Ultimate 3000 RSLC system (Thermo Fisher Scientific, Hemel
694 Hempstead, UK). Samples were separated on a Luna Omega Polar C18 column (150×2.1 mm i.d., 1.6
695 µm, Phenomenex, Sartrouville, France) equipped with a guard column. The mobile phase A (MPA) was
696 H_2O with 0.05% formic acid (FA) and the mobile phase B (MPB) was CH_3CN with 0.05% FA. The solvent
697 gradient started with 2% B for 30 s, reaching 70% B at 10.5 min and 98% at 10.6 min, holding 98% for
698 2 min, and coming back to the initial condition of 2% B in 0.1 min, for a total run time of 14 min. The
699 flow rate was 0.3 $mL.min^{-1}$, the column temperature was set to 40 °C, the autosampler temperature
700 was set to 10 °C, and the injection volume was fixed at 2 µL. Mass detection was performed in positive
701 ionization (PI) and negative ionization (NI) modes at 30 000 resolving power [full width at half
702 maximum (FWHM) at 400 m/z] for MS1 and 17 500 for MS2 with an automatic gain control (AGC)
703 target of 10^{-5}. Ionization spray voltages were set to 3.5 kV (for PI) and 2.5 kV (for NI) and the capillary

704 temperature was set to 256°C for both modes. The mass scanning range was m/z 100-1500 Da. Each
705 full MS scan was followed by data-dependent acquisition of MS/MS data for the six most intense ions
706 using stepped normalized collision energy of 20, 40, and 60 eV.

707 The raw data were processed with MS-DIAL version 4.70 for mass signal extraction between 100
708 and 1,500 Da from 0.5 to 10.6 min, respectively[73,74]. MS1 and MS2 tolerance were set to 0.01 and
709 0.025 Da in the centroid mode. The optimized detection threshold was set to 5×10^5 concerning MS1
710 and 10 for MS2. Peaks were aligned on a QC reference file with a retention time tolerance of 0.15 min
711 and a mass tolerance of 0.015 Da. Minimum peak height was set to 70% below the observed total ion
712 chromatogram (TIC) baseline for a blank injection. Peak annotation was performed with an in-house
713 database built on an MS-FINDER model[73].

714 MS-DIAL data were then cleaned with the MS-CleanR workflow by selecting all filters with a
715 minimum blank ratio set to 0.8, a maximum relative standard deviation (RSD) set to 30, and a relative
716 mass defect (RMD) ranging from 50 to 3,000. The maximum mass difference for feature relationships
717 detection was set to 0.005 Da and the maximum RT difference to 0.025 min. Pearson correlation links
718 were considered with correlation ≥ 0.8 and statistically significant with $\alpha = 0.05$. Two peaks were kept
719 in each cluster*, viz.,* the most intense and the most connected. The kept features (m/z × RT pairs) were
720 annotated with MS-FINDER version 3.52. The MS1 and MS2 tolerances were, respectively, set to 10
721 and 20 ppm. Formula finders were only processed with C, H, O, N, and S atoms. Databases (DBs) based
722 on *Arabidopsis* (genus), *Brassicaceae* (family), and *Streptomyces* (genus of the AgN23 strain), were
723 constituted with the dictionary of natural products (DNP, CRC press, DNP on DVD v. 28.2). The internal
724 generic DBs from MS-FINDER used were KNApSAcK, PlantCyc, NANPDB, UNPD, COCONUT, and CheBI.
725 Annotation prioritization was done by ranking *Arabidopsis* DB, followed by *Brassicaceae* DB,
726 *Streptomyces* DB, and finally generic DBs using the final MS-CleanR step.

727 Statistical analyses were done by using SIMCA (version 14.1, Umerics). All data were scaled by
728 pareto scaling before multivariate analysis. The (orthogonal) projection to latent structure using

729 discriminant analysis ((O)PLS-DA) was used to separate data according to *A. thaliana* growing
730 conditions. Variable Importance in Projection (VIP) features were selected according to their VIP score
731 (>3). The principal component analysis was built with the web-interface MetaboAnalyst version 5.0
732 (http://www.metaboanalyst.ca)[75]. Significantly different metabolites and affiliated chemical classes
733 with ClassyFire were selected using the criteria of $p < 0.05$ (t-test, control vs. treatment, unadjusted
734 p-value) and log2 fold change (log2FC) > 0.8 or < -0.8[76].

735 **Microscopy**

736 For stereo microscopy, we used a Nikon SMZ16 microscope equipped with a camera. Confocal
737 microscopy was performed on a TCS SP8 confocal microscope (Leica, Microsystems, UK). For GFP-
738 tagged AgN23 cells, the excitation wavelength was 488 nm, with emission absorbance between 500
739 nm and 550 nm, whereas an excitation wavelength of 543 nm was used for mCherry-tagged AgN23
740 cells proteins, with emission absorbance between 560 nm and 600 nm. Images were acquired with a
741 ×40 or ×20 water immersion lens. All confocal images were analysed and processed using the ImageJ
742 software package (http://rsb.info.nih.gov/ij/; v. 1.51k).

743 **Antifungal activity**

744 For the determination of AgN23 CME IC_{50} against fungi, the *Botrytis cinerea* BD90 strain was cultivated
745 onto solid Potato Dextrose Agar (39 g/L, Sigma). Fungal spores were harvested 8 days after cultivation
746 by pouring 5 mL of sterile ultrapure water into the plate and gently scrapping the surface with a sterile
747 spreader. Spores were counted on a Fuchs-Rosenthal cell and the spore suspension was adjusted to
748 5555 spores/mL in Potato Dextrose Broth (5.3 g/L, Sigma). 90 µL of spore suspension were distributed
749 in 96-well plates. 10 µL of culture supernatant extracts from AgN23 WT of AgN23 KO mutants at
750 different concentrations (20–100 µg dry extracts/mL) were added with 3 replicates per concentration.
751 *B. cinerea* growth was monitored by OD_{600} readings with an ELx808TM Incubating Absorbance
752 Microplate Reader (Bio-Tek) 0, 3, and 6 days after treatment. Growth inhibition (I) was calculated as:

753 $$I = \frac{OD_T - OD_{T0}}{OD_{TControl} - OD_{T0Control}}$$

754 Where OD_T is OD_{600} of treatment condition at time = T, OD_{T0} is OD_{600} of treatment condition at time =
755 T0, $OD_{TControl}$ is OD_{600} of control condition at time = T, OD_{T0} is OD_{600} of control condition at time = T0.

756 ***Arabidopsis* Inositol Phosphorylceramide Synthase inhibition assay**

757 To study the effect of AgN23 CME on *Arabidopsis* IPCs, we purified microsomal fractions of transgenic
758 yeast expressing AtIPCS2 (AT2G37940) in enzymatic activity assays. First, a preculture of yeast MSY23-
759 3C pESC-LEU_AtIPCS2 strain was performed by picking a single colony and propagating it in 5 mL SGR
760 -TRP -LEU medium (0.1% galactose, 1% raffinose) [37]. The preculture was incubated at 30 °C, 200 rpm
761 until the OD_{600} reached 0.8. The preculture was then mixed with 245 mL of fresh SGR medium and
762 incubated at 30 °C, 200 rpm until the OD_{600} reached 0.8. Yeast cells were then harvested by
763 centrifugation, washed with cold phosphate-buffered saline, and stored at -80 °C until microsome
764 preparation. Crude microsomal membranes from yeast MSY23-3C pESC-LEU_AtIPCS2 strain were
765 prepared as previously described with additional CHAPSO washing steps[77]. Total protein quantification
766 was performed by Bradford assay and aliquots at 0.5 mg/mL were made and stocked at -80 °C.

767 AtIPCS2 activity assays were performed following a fluorometric assay as described earlier[38]. The
768 Initial velocities of the AtIPCS2 reaction were measured at various NBD-C6-phytoceramide (2.5 – 80
769 µM, final concentration, Cayman) with a fixed soybean PI concentration (2 mM, final concentration,
770 Sigma) and a total microsomal proteins concentration of 0.1 mg/mL. Enzymatic reactions (50 µL final
771 volume) were done in 2 mL microtubes and incubated at 30 °C for 30 min. Following incubation, the
772 reactions were quenched with 150 µL methanol. After centrifugation at 10,000 g for 3 min, the organic
773 phase was removed, dried under nitrogen flow, and re-suspended in 100 µL methanol. 15 µL
774 quantities were injected using an automatic sample injector into the HPLC instrument. The fluorescent
775 substrate and product (V_{ex} = 465 nm, V_{em} = 530 nm) were separated on a XBridge C18 reversed-phase
776 column (Waters) with the following gradient at 1 mL/min: 50% CH_3CN – 50% H_2O – 0.1% CH_3COOH to

90% CH_3CN – 10% H_2O – 0.1% CH_3COOH. Two HPLC peaks were observed for the substrate and reaction product at 13.8 and 4.1 minutes, respectively. 15 µL quantities of NBD-C6-phytoceramide at known concentrations were injected to the calculate AtIPCS2 velocity. As the substrate fluorescence is equal to the product fluorescence, the enzyme velocity was determined as the rate of product formation over time. Data were fitted to the Michaelis-Menten equation and the apparent Km and Vmax were estimated to be 7.57 µM and 0.01 mol/min/mg of protein, respectively.

TABLE

Table 1: List of detected metabolites with highest intensities on chromatogram

Peak name	Ret. Time (min)	m/z
Galbonolide E	7.63	365.19
Galbonolide A	7.92	379.21
Galbonolide G	8.21	363.21
Niphimycin	8.53	1140.71
Niphimycin	9.15	1140.71
Nigericin	12.417	723.47
Nigericin	15.12	723.47

Table 2: 50% inhibitory concentration (IC_{50}) of AgN23 WT and KO mutants (pSC004) CME against *Botrytis cinerea.* Table shows mean ± SD calculated from six biological replicates (n = 6)

Strain	IC_{50} (µg/mL)
AgN23 WT	33.28 ± 0.20
pSC004-1	48.06 ± 1.68

pSC004-10	47.27 ± 1.29
pSC004-16	46.13 ± 1.29
pSC004-22	54.42 ± 3.7

REFERENCE

1 Mendes, R. & Raaijmakers, J. M. Cross-kingdom similarities in microbiome functions. *The ISME Journal* **9**, 1905-1907 (2015). https://doi.org/10.1038/ismej.2015.7

2 Getzke, F. *et al.* Cofunctioning of bacterial exometabolites drives root microbiota establishment. *Proceedings of the National Academy of Sciences* **120**, e2221508120 (2023). https://doi.org/10.1073/pnas.2221508120

3 Krespach, M. K. C. *et al.* Streptomyces polyketides mediate bacteria–fungi interactions across soil environments. *Nature Microbiology* **8**, 1348-1361 (2023). https://doi.org/10.1038/s41564-023-01382-2

4 Krespach, M. K. C. *et al.* Bacterial marginolactones trigger formation of algal gloeocapsoids, protective aggregates on the verge of multicellularity. *Proceedings of the National Academy of Sciences* **118**, e2100892118 (2021). https://doi.org/10.1073/pnas.2100892118

5 Andrić, S. *et al.* Plant-associated Bacillus mobilizes its secondary metabolites upon perception of the siderophore pyochelin produced by a Pseudomonas competitor. *ISME J* **17**, 263-275 (2023). https://doi.org/10.1038/s41396-022-01337-1

6 Andrić, S. *et al.* Lipopeptide Interplay Mediates Molecular Interactions between Soil Bacilli and Pseudomonads. *Microbiol Spectr* **9**, e0203821 (2021). https://doi.org/10.1128/spectrum.02038-21

7 Fitzpatrick, C. R. *et al.* Assembly and ecological function of the root microbiome across angiosperm plant species. *Proc Natl Acad Sci U S A* **115**, E1157-E1165 (2018). https://doi.org/10.1073/pnas.1717617115

8 Durán, P. *et al.* Microbial Interkingdom Interactions in Roots Promote *Arabidopsis* Survival. *Cell* **175**, 973-983.e914 (2018). https://doi.org/10.1016/j.cell.2018.10.020

9 Chaparro, J. M., Badri, D. V. & Vivanco, J. M. Rhizosphere microbiome assemblage is affected by plant development. *ISME J* **8**, 790-803 (2014). https://doi.org/10.1038/ismej.2013.196

10 Fitzpatrick, C. R. *et al.* The Plant Microbiome: From Ecology to Reductionism and Beyond. *Annu Rev Microbiol* (2020). https://doi.org/10.1146/annurev-micro-022620-014327

11 Thiergart, T. *et al.* Root microbiota assembly and adaptive differentiation among European *Arabidopsis* populations. *Nat Ecol Evol* **4**, 122-131 (2020). https://doi.org/10.1038/s41559-019-1063-3

12 Russ, D., Fitzpatrick, C. R., Teixeira, P. J. P. L. & Dangl, J. L. Deep discovery informs difficult deployment in plant microbiome science. *Cell* **186**, 4496-4513 (2023). https://doi.org/10.1016/j.cell.2023.08.035

13 Busby, P. E. *et al.* Research priorities for harnessing plant microbiomes in sustainable agriculture. *PLoS Biol* **15**, e2001793 (2017). https://doi.org/10.1371/journal.pbio.2001793

14 Berendsen, R. L. *et al.* Disease-induced assemblage of a plant-beneficial bacterial consortium. *ISME J* **12**, 1496-1507 (2018). https://doi.org/10.1038/s41396-018-0093-1

15 Yang, Z. *et al.* Streptomyces alleviate abiotic stress in plant by producing pteridic acids. *Nature Communications* **14**, 7398 (2023). https://doi.org/10.1038/s41467-023-43177-3

16 Lebeis, S. L. *et al.* PLANT MICROBIOME. Salicylic acid modulates colonization of the root microbiome by specific bacterial taxa. *Science* **349**, 860-864 (2015). https://doi.org/10.1126/science.aaa8764

17 Bulgarelli, D. *et al.* Revealing structure and assembly cues for *Arabidopsis* root-inhabiting bacterial microbiota. *Nature* **488**, 91-95 (2012). https://doi.org/10.1038/nature11336

18 Lundberg, D. S. *et al.* Defining the core *Arabidopsis* thaliana root microbiome. *Nature* **488**, 86-90 (2012). https://doi.org/10.1038/nature11237

19 Cha, J. Y. *et al.* Microbial and biochemical basis of a Fusarium wilt-suppressive soil. *ISME J* **10**, 119-129 (2016). https://doi.org/10.1038/ismej.2015.95

20 Kim, D. R. *et al.* A mutualistic interaction between Streptomyces bacteria, strawberry plants and pollinating bees. *Nat Commun* **10**, 4802 (2019). https://doi.org/10.1038/s41467-019-12785-3

21 Cordovez, V. *et al.* Diversity and functions of volatile organic compounds produced by Streptomyces from a disease-suppressive soil. *Front Microbiol* **6**, 1081 (2015). https://doi.org/10.3389/fmicb.2015.01081

22 Avalos, M., Garbeva, P., Raaijmakers, J. M. & van Wezel, G. P. Production of ammonia as a low-cost and long-distance antibiotic strategy by Streptomyces species. *ISME J* **14**, 569-583 (2020). https://doi.org/10.1038/s41396-019-0537-2

23 Conn, V. M., Walker, A. R. & Franco, C. M. Endophytic actinobacteria induce defense pathways in *Arabidopsis thaliana*. *Mol Plant Microbe Interact* **21**, 208-218 (2008). https://doi.org/10.1094/MPMI-21-2-0208

24 Kurth, F. *et al.* Streptomyces-induced resistance against oak powdery mildew involves host plant responses in defense, photosynthesis, and secondary metabolism pathways. *Mol Plant Microbe Interact* **27**, 891-900 (2014). https://doi.org/10.1094/MPMI-10-13-0296-R

25 Rey, T. & Dumas, B. Plenty Is No Plague: Streptomyces Symbiosis with Crops. *Trends Plant Sci* **22**, 30-37 (2017). https://doi.org/10.1016/j.tplants.2016.10.008

26 Viaene, T., Langendries, S., Beirinckx, S., Maes, M. & Goormachtig, S. Streptomyces as a plant's best friend? *FEMS Microbiol Ecol* **92** (2016). https://doi.org/10.1093/femsec/fiw119

27 Vergnes, M. S. *et al.* Phyllosphere colonisation by a soil Streptomyces sp. promotes plant defense responses against fungal infection. 43 (2020).

28 Gayrard, D. *et al.* Genome Sequence of the Streptomyces Strain AgN23 Revealed Expansion and Acquisition of Gene Repertoires Potentially Involved in Biocontrol Activity and Rhizosphere Colonization. *PhytoFrontiers™*, PHYTOFR-11-22-0131-R (2023). https://doi.org/10.1094/PHYTOFR-11-22-0131-R

29 Schuhegger, R. *et al.* CYP71B15 (PAD3) Catalyzes the Final Step in Camalexin Biosynthesis. *Plant Physiology* **141**, 1248-1254 (2006). https://doi.org/10.1104/pp.106.082024

30 Bromley, P. E., Li, Y. O., Murphy, S. M., Sumner, C. M. & Lynch, D. V. Complex sphingolipid synthesis in plants: characterization of inositolphosphorylceramide synthase activity in bean microsomes. *Arch Biochem Biophys* **417**, 219-226 (2003).

31 Zeng, H.-Y. *et al.* The Two Classes of Ceramide Synthases Play Different Roles in Plant Immunity and Cell Death. *Frontiers in Plant Science* **13**, 824585 (2022). https://doi.org/10.3389/fpls.2022.824585

32 König, S. *et al.* Sphingolipid-Induced Programmed Cell Death is a Salicylic Acid and EDS1-Dependent Phenotype in Arabidopsis fatty acid hydroxylase (fah1, fah2) and ceramide synthase (loh2) Triple Mutants. *Plant Cell Physiol* (2021). https://doi.org/10.1093/pcp/pcab174

33 Zienkiewicz, A. *et al.* Disruption of Arabidopsis neutral ceramidases 1 and 2 results in specific sphingolipid imbalances triggering different phytohormone-dependent plant cell death programmes. *New Phytol* **226**, 170-188 (2020). https://doi.org/10.1111/nph.16336

34 Luttgeharm, K. D. *et al.* Overexpression of Arabidopsis Ceramide Synthases Differentially Affects Growth, Sphingolipid Metabolism, Programmed Cell Death, and Mycotoxin Resistance. *Plant Physiol* **169**, 1108-1117 (2015). https://doi.org/10.1104/pp.15.00987

35 Ternes, P. *et al.* Disruption of the ceramide synthase LOH1 causes spontaneous cell death in Arabidopsis thaliana. *New Phytologist* **192**, 841-854 (2011). https://doi.org/10.1111/j.1469-8137.2011.03852.x

36 Wang, W. *et al.* An inositolphosphorylceramide synthase is involved in regulation of plant programmed cell death associated with defense in Arabidopsis. *Plant Cell* **20**, 3163-3179 (2008). https://doi.org/10.1105/tpc.108.060053

37 Pinneh, E. C. *et al.* The identification of small molecule inhibitors of the plant inositol phosphorylceramide synthase which demonstrate herbicidal activity. *Sci Rep* **9**, 8083 (2019). https://doi.org/10.1038/s41598-019-44544-1

38 Zhong, W., Murphy, D. J. & Georgopapadakou, N. H. Inhibition of yeast inositol phosphorylceramide synthase by aureobasidin A measured by a fluorometric assay. *FEBS Letters*, 4 (1999).

39 Takatsu, T. *et al.* Rustmicin, a new macrolide antibiotic active against wheat stem rust fungus. *J Antibiot (Tokyo)* **38**, 1806-1809 (1985).

40 Harris, G. H. *et al.* Inhibition of fungal sphingolipid biosynthesis by rustmicin, galbonolide B and their new 21-hydroxy analogs. *J Antibiot (Tokyo)* **51**, 837-844 (1998).

41 Lachaud, C. *et al.* Nuclear calcium controls the apoptotic-like cell death induced by d-erythro-sphinganine in tobacco cells. *Cell Calcium* **47**, 92-100 (2010). https://doi.org/10.1016/j.ceca.2009.11.011

42 He, Z., Webster, S. & He, S. Y. Growth–defense trade-offs in plants. *Current Biology* **32**, R634-R639 (2022). https://doi.org/10.1016/j.cub.2022.04.070

43 Nguyen, N. H. *et al.* Camalexin accumulation as a component of plant immunity during interactions with pathogens and beneficial microbes. *Planta* **255**, 116 (2022). https://doi.org/10.1007/s00425-022-03907-1

44 Wolinska, K. W. *et al.* Tryptophan metabolism and bacterial commensals prevent fungal dysbiosis in Arabidopsis roots. *Proceedings of the National Academy of Sciences* **118**, e2111521118 (2021). https://doi.org/10.1073/pnas.2111521118

45 Korenblum, E. *et al.* Rhizosphere microbiome mediates systemic root metabolite exudation by root-to-root signaling. *Proceedings of the National Academy of Sciences* **117**, 3874-3883 (2020). https://doi.org/10.1073/pnas.1912130117

46 Stringlis, I. A. *et al.* MYB72-dependent coumarin exudation shapes root microbiome assembly to promote plant health. *Proceedings of the National Academy of Sciences* **115**, E5213-E5222 (2018). https://doi.org/10.1073/pnas.1722335115

47 Stringlis, I. A. *et al.* Root transcriptional dynamics induced by beneficial rhizobacteria and microbial immune elicitors reveal signatures of adaptation to mutualists. *Plant J* **93**, 166-180 (2018). https://doi.org/10.1111/tpj.13741

48 Harbort, C. J. *et al.* Root-Secreted Coumarins and the Microbiota Interact to Improve Iron Nutrition in Arabidopsis. *Cell Host & Microbe* **0** (2020). https://doi.org/10.1016/j.chom.2020.09.006

49 Voges, M. J. E. E. E., Bai, Y., Schulze-Lefert, P. & Sattely, E. S. Plant-derived coumarins shape the composition of an Arabidopsis synthetic root microbiome. *Proceedings of the National Academy of Sciences* **116**, 12558-12565 (2019). https://doi.org/10.1073/pnas.1820691116

50 Singh, G., Agrawal, H. & Bednarek, P. Specialized metabolites as versatile tools in shaping plant–microbe associations. *Molecular Plant* **16**, 122-144 (2023). https://doi.org/10.1016/j.molp.2022.12.006

51 Koprivova, A., Schwier, M., Volz, V. & Kopriva, S. Shoot-root interaction in control of camalexin exudation in Arabidopsis. *J Exp Bot* **74**, 2667-2679 (2023). https://doi.org/10.1093/jxb/erad031

52 Koprivova, A. *et al.* Root-specific camalexin biosynthesis controls the plant growth-promoting effects of multiple bacterial strains. *Proceedings of the National Academy of Sciences* **116**, 15735-15744 (2019). https://doi.org/10.1073/pnas.1818604116

53 Berkey, R., Bendigeri, D. & Xiao, S. Sphingolipids and Plant Defense/Disease: The "Death" Connection and Beyond. *Frontiers in Plant Science* **3**, 68 (2012). https://doi.org/10.3389/fpls.2012.00068

54 Kim, H. J. *et al.* A single module type I polyketide synthase directs de novo macrolactone biogenesis during galbonolide biosynthesis in Streptomyces galbus. *J Biol Chem* **289**, 34557-34568 (2014). https://doi.org/10.1074/jbc.M114.602334

55 Liu, C., Zhang, J., Lu, C. & Shen, Y. Heterologous expression of galbonolide biosynthetic genes in Streptomyces coelicolor. *Antonie van Leeuwenhoek* **107**, 1359-1366 (2015). https://doi.org/10.1007/s10482-015-0415-5

56 Liu, C. *et al.* In Vitro Reconstitution of a PKS Pathway for the Biosynthesis of Galbonolides in Streptomyces sp. LZ35. *ChemBioChem* **16**, 998-1007 (2015). https://doi.org/10.1002/cbic.201500017

57 Karki, S. *et al.* The methoxymalonyl-acyl carrier protein biosynthesis locus and the nearby gene with the beta-ketoacyl synthase domain are involved in the biosynthesis of galbonolides in Streptomyces galbus, but these loci are separate from the modular polyketide synthase gene cluster. *FEMS Microbiol Lett* **310**, 69-75 (2010). https://doi.org/10.1111/j.1574-6968.2010.02048.x

58 Shafiee, A. *et al.* Microbial hydroxylation of rustmicin (galbonolide A) and galbonolide B, two antifungal products produced by Micromonospora sp. *Journal of Molecular Catalysis B: Enzymatic* **11**, 237-242 (2001). https://doi.org/10.1016/S1381-1177(00)00067-9

59 Sigmund, J. M. & Hirsch, C. F. Fermentation studies of rustmicin production by a Micromonospora sp. *J Antibiot (Tokyo)* **51**, 829-836 (1998).

60 Mandala, S. M. *et al.* Rustmicin, a potent antifungal agent, inhibits sphingolipid synthesis at inositol phosphoceramide synthase. *J Biol Chem* **273**, 14942-14949 (1998).

61 Nakayama, H. *et al.* Structures of neorustmicins B, C and D new congeners of rustmicin and neorustmicin A. *J Antibiot (Tokyo)* **39**, 1016-1020 (1986).

62 Achenbach, H., Mühlenfeld, A., Fauth, U. & Zähner, H. The galbonolides. Novel, powerful antifungal macrolides from Streptomyces galbus ssp. eurythermus. *Ann N Y Acad Sci* **544**, 128-140 (1988).

63 Fauth, U., Zähner, H., Mühlenfeld, A. & Achenbach, H. Galbonolides A and B--two non-glycosidic antifungal macrolides. *J Antibiot (Tokyo)* **39**, 1760-1764 (1986).

64 Bromley, P. E., Li, Y. O., Murphy, S. M., Sumner, C. M. & Lynch, D. V. Complex sphingolipid synthesis in plants: characterization of inositolphosphorylceramide synthase activity in bean microsomes. *Archives of Biochemistry and Biophysics* **417**, 219-226 (2003). https://doi.org/10.1016/S0003-9861(03)00339-4

65 Iqbal, N., Czékus, Z., Poór, P. & Ördög, A. Plant defence mechanisms against mycotoxin Fumonisin B1. *Chem Biol Interact* **343**, 109494 (2021). https://doi.org/10.1016/j.cbi.2021.109494

66 Zeng, H. Y., Li, C. Y. & Yao, N. Fumonisin B1: A Tool for Exploring the Multiple Functions of Sphingolipids in Plants. *Front Plant Sci* **11**, 600458 (2020). https://doi.org/10.3389/fpls.2020.600458

67 Pinneh, E. C. *Targeting a promising new herbicide mode of action: chemical and genetic approaches to elucidate the role of IPC synthase in plants*, Durham University, (2017).

68 Pauly, N. *et al.* The nucleus together with the cytosol generates patterns of specific cellular calcium signatures in tobacco suspension culture cells. *Cell Calcium* **30**, 413-421 (2001). https://doi.org/10.1054/ceca.2001.0250

69 Clough, S. J. & Bent, A. F. Floral dip: a simplified method for Agrobacterium-mediated transformation of Arabidopsis thaliana. *Plant J* **16**, 735-743 (1998). https://doi.org/10.1046/j.1365-313x.1998.00343.x

70 Johansson, O. N. *et al.* A quick and robust method for quantification of the hypersensitive response in plants. *PeerJ* **3**, e1469 (2015). https://doi.org/10.7717/peerj.1469

71 Mithöfer, A., Mazars, C. & Maffei, M. E. in *Plant Signal Transduction: Methods and Protocols Methods in Molecular Biology* (ed Thomas Pfannschmidt) 79-92 (Humana Press, 2009).

72 Allen, D. G., Blinks, J. R. & Prendergast, F. G. Aequorin Luminescence: Relation of Light Emission to Calcium Concentration-A Calcium-Independent Component. *Science* **195**, 996-998 (1977).

73 Fraisier-Vannier, O. *et al.* MS-CleanR: A feature-filtering approach to improve annotation rate in untargeted LC-MS based metabolomics. (Bioinformatics, 2020).

74 Tsugawa, H. *et al.* MS-DIAL: data-independent MS/MS deconvolution for comprehensive metabolome analysis. *Nature Methods* **12**, 523-526 (2015). https://doi.org/10.1038/nmeth.3393

75 Pang, Z. *et al.* MetaboAnalyst 5.0: narrowing the gap between raw spectra and functional insights. *Nucleic Acids Research* **49**, W388-W396 (2021). https://doi.org/10.1093/nar/gkab382

76 Djoumbou Feunang, Y. *et al.* ClassyFire: automated chemical classification with a comprehensive, computable taxonomy. *Journal of Cheminformatics* **8**, 61 (2016). https://doi.org/10.1186/s13321-016-0174-y

77 Mina, J. G. *et al.* Functional analyses of differentially expressed isoforms of the Arabidopsis inositol phosphorylceramide synthase. *Plant Mol Biol* **73**, 399-407 (2010). https://doi.org/10.1007/s11103-010-9626-3